CHALMERS

Estimation of the absorption of extraterrestrial radio noise using a narrow beam VHF radar at 53.5 MHz in Andenes, Norway

Master of Science Thesis

SEYED SOHEIL SADEGHI

Department of Radio and Space Science
CHALMERS UNIVERSITY OF TECHNOLOGY
Göteborg, Sweden, 2008

Estimation of the absorption of extraterrestrial radio noise using a narrow beam VHF radar at 53.5 MHz in Andenes, Norway

SEYED SOHEIL SADEGHI

LEIBNIZ-INSTITUT FÜR ATMOSPHÄREN PHYSIK IAP

Leibniz Institute of Atmospheric Physics (IAP)
Kühlungsborn, Germany

Department of Radio and Space Science
CHALMERS UNIVERSITY OF TECHNOLOGY

Göteborg, Sweden, 2008

Estimation of the absorption of extraterrestrial radio noise using a narrow beam VHF radar at 53.5 MHz in Andenes, Norway

Supervisor:
Dr. Werner Singer
Leibniz Institute of Atmospheric Physics (IAP)
Kühlungsborn, Germany

Examiner:
Dr. Leif Eriksson
Department of Radio and Space Science
Chalmers University of Technology
SE-412 96 Göteborg
Sweden
Telephone: +46 (0)31-772 1000

Göteborg, Sweden, 2008

Estimation of the absorption of extraterrestrial radio noise using a narrow beam VHF radar at 53.5 MHz in Andenes, Norway

SEYED SOHEIL SADEGHI

Department of Radio and Space Science

Chalmers University of Technology

Abstract

The Earth's magnetic field works like a shield against the solar wind flux of plasma, but at the polar regions, where it fails to do so, these charged particles may be guided down to low altitudes and introduce a lot of impacts on the environment, ranging from the nice colourful Aurora, to chemical changes in the atmosphere and decrease in the amount of ozone in the middle atmosphere, and from satellite damages to power line cut offs, depending on the type and energy of the particles.

Extraterrestrial HF/VHF radio noise from the universe and mainly from our own galaxy is continuously coming towards our planet. Absorption of these electromagnetic waves in the Earth's ionosphere is a well known proxy of the events which can enhance it, mainly having direct or indirect root in the solar activities, like Solar Flares, Coronal Mass Ejections, and Geomagnetic Storms and the resulted X rays, Solar Proton Events and Precipitating Energetic charged Particles.

Cosmic radio noise power and the corresponding ionospheric absorption is normally measured by the riometers (Relative Ionospheric Opacity Meters for Extraterrestrial Electromagnetic Radiation), and especially in recent years by multiple narrow beam imaging riometers.

In this thesis, the data obtained by the vertical beam of a narrow beam MST radar, ALWIN, at Andenes, Norway (69.17°N; 16.01°E) is used as a (narrow beam of a) riometer to estimate the incident cosmic noise power at 53.5 MHz and its absorption, especially during solar/geomagnetic activity periods. The results are in good agreement with riometers (IRIS and AIRIS in Andenes and Kilpisjarvi Finland, 69.06°N, 20.55°E) common volume measurements and with electron density measurements of the Saura MF Radar. The obtained Quiet Day Curves (QDCs) are in very good agreement with theoretical and observed QDCs estimated by Friedrich et al. (2001).

Keywords: ionosphere, cosmic radio noise, absorption, solar activity, riometer, radar

Contents

Acknowledgements

This thesis was performed at the Leibniz Institute for Atmospheric Physics, IAP, Kühlungsborn, Germany. I thank my supervisor, Dr. Werner Singer so much and I owe him for ever for his invaluable support and guidance.

I am grateful to my examiner, Dr. Leif Eriksson, very much for his comments and follow-up of the thesis steps; and to all people at Radio and Space Science group at Chalmers.

My special thanks go to professor Franz-Josef Lübken and to all IAP colleagues, especially professor Markus Rapp, Dr. Norbert Engler, and Dr. Marius Zecha.

The Riometer data and maps were obtained from Lancaster University, thanks to Dr. Steve Marple.

The master's thesis project included a 10-day stay at Andoya Rocket Range in Norway and was presented in the eARI ALOMAR users' meeting 19-23 May 2008, Nessebar, Bulgaria, funded by the Europian Union; I am indebted to the personnel of ARR for their hospitality during my stay at ARR and in Nessebar.

Soheil Sadeghi

Göteborg, June 2008

Abbreviations and acronyms

-A2 Method: Cosmic Noise Absorption Method of Ionospheric Absorption measurement
-AIRIS: Andoya Imaging Riometer for Ionospheric Studies
-ALOMAR: Arctic Lidar Observatory for Middle Atmosphere Research
-ALWIN: ALOMAR Wind radar
-Andenes: name (of site place, 69.17°N; 16.01°E)
-ARR: Andoya Rocket Range
-CNA: Cosmic Noise Absorption
-CNP: Cosmic Noise Power
-DAE: Differential Absorption Electron density measurements
-DBS: Doppler Beam Swinging
-DPE: Differential Phase Electron density measurements
-GOES satellite: The Geostationary Operational Environmental Satellite program
-GOES SEM: GOES Space Environment Monitor
-IAP: Leibniz Institute for Atmospheric Physics (Kuehlungsborn-Germany)
-IRIS: Imaging Riometer for Ionospheric Studies (In this thesis IRIS name is used for the Kilpisjarvi IRIS Riometer; unless otherwise mentioned)
-I, Q Signals of Radars: In_Phase and Quadrature_Phase voltage components of a Radar voltage signal, i(t) and q(t)
-Kilpisjarvi-Finland: name (of site place, 69.06°N; 20.55°E)
-MF: Medium Frequency
-MST Radar: Mesospheric Stratospheric Tropospheric Radar .
-PCA: Polar Cap Absorption
-QDC: Quiet-Day-Curve:
-Riometer: Relative Ionospheric Opacity Meter (for ExtraTerrestrial Electromagnetic Radiation)
-RNP: Radio Noise Power
-SA method: Spaced Antenna method
-Saura: name (of site place 69.14°N; 16.01°E)
-SID: Sudden Ionospheric Disturbance
-SPE: Solar Proton Event
-ST: Sidereal Time
-Tromsö: name (of site place, 69.68°N; 18.94.°E)
-UT: Universal time
-WMA: Weighted Moving Average

1. Introduction

Radio noise of extraterrestrial origin is continuously incident on the top of the ionosphere over a wide range of frequencies. In the upper HF and lower VHF bands the major contribution to the cosmic noise comes from our own galaxy. Smaller contributions are due to the more intense discrete sources of both galactic and extragalactic origin and to the sun. The galactic radio noise received with the usual antenna beams at a given sidereal time does not vary with time in general. Therefore the cosmic radio noise power curve measured with a fixed receiving system on the Earth ought to be constant if there was no absorption in the Earth's ionosphere [Rawer, 1976]. This is the main idea behind riometer experiment which expects that a non attenuated amount of cosmic noise power exists (for each sidereal time, at a receiver site) as a reference, to which the attenuated power can be compared in order to measure/estimate the absorption. The cosmic radio noise power is a reliable indicator of the integrated absorption produced by the ionosphere if the instantaneous measured value is compared with the quiet background signal. Absorption in an ionized medium is due to energy transfer of the wave to electrons and loss of the energy in collisions between electrons and other particles. The energy loss, therefore, depends on the number of available particles for collisions and hence the number of collision partners (mainly neutrals). At high altitudes the very small neutral density does not provide enough collision partners; at low altitudes the electron densities are too low; hence, between these extremes there exists a height region where the likelihood for energy loss (by collisions between electrons with motions ordered by the incident wave and neutrals) maximises. This maximum is generally between 70 and 100 km [Friedrich et al. 2001].

The measurement of cosmic radio noise absorption is ideally suited for the study of excess absorption events occurring especially at high latitudes under disturbed conditions (solar flares/X rays, coronal mass ejections/solar proton events, geomagnetic storms/precipitating high energetic particles) [Rawer, 1976].

For studies of the dynamics and structure of precipitating particles the AIRIS system (Andoya Imaging Riometer for Ionospheric Studies, http://alomar.rocketrange.no/iris-and.html) is in operation in Andenes, Norway (69.17°N; 16.01°E) since January 2006 at 38.2 MHz. In addition, the IAP continuously operates the ALWIN MST radar at 53.5 MHz at the same site. The ALWIN system acquires data at a wide height range, at heights where atmospheric/ionospheric signals are present (where the ionization exists, i.e. higher than 65 km) and at heights where the radio noise power is measured alone (20 to 60 km). Solar activity can lead to enhanced ionization at lower altitudes, even down to 54 km (and far lower) , and hence stronger radar signals at these heights.

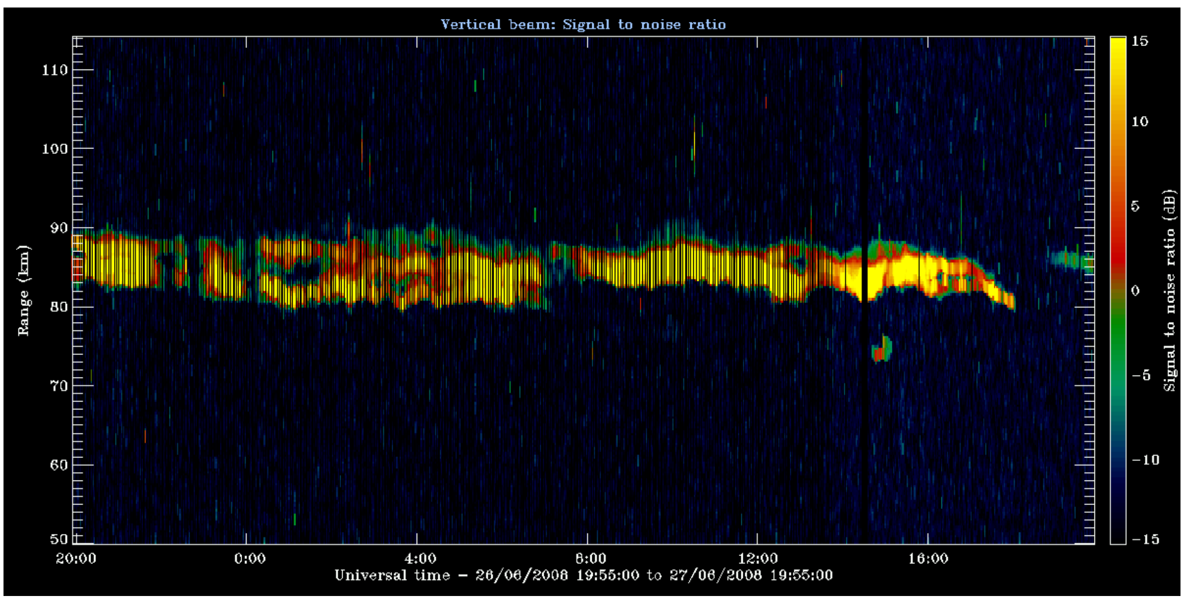

Fig. 1.1. Signal-to-Noise Ratio for the Vertical Beam of ALWIN Radar at height range 50 to 110 km during 24 hours in 26 June 2008, illustrating the normal peak of the echoes at around 85 km.

In this thesis, the radio noise power data (at 53.5 MHz) from ALWIN MST radar, from 50 to 54km heights is used to estimate the (attenuated and non attenuated) cosmic radio noise power. The results obtained for the vertical antenna beam are compared with the corresponding beams of riometers AIRIS and IRIS and the D-region electron number densities estimated from the Saura MF radar on Andoya.

Outline of the thesis

Chapter 2 deals briefly with the atmosphere, the ionosphere, sources of ionization and ionization enhancement, and the impacts of solar and geomagnetic activities. Chapter 3 provides an overview of the sources of radio noise and the mechanism of the ionospheric radio noise absorption and the ionization observation instruments used in this thesis. The method used to obtain the cosmic radio noise and its ionospheric absorption from ALWIN observations is explained in chapter 4. In chapter 5, the obtained results are presented and compared with the common-volume results of riometers and other observations. Discussions, summary, and possible further investigations will be presented in chapter 6.

2. The upper atmosphere of the Earth

The atmosphere of the Earth is an ocean of gas encircling the globe. It stretches out into far distances from the surface; becomes thinner exponentially and fades into space. The atmosphere protects life on Earth by absorbing ultraviolet solar radiation and reducing temperature extremes between day and night. Three quarters of the atmosphere's mass is within 11 km of the planetary surface.

The upper polar atmosphere sets the scene for one of the natures amazing celestial phenomena, the Aurora borealis, the colourful, dynamical forms are the end product of a long chain of plasma processes initiated by particle eruptions on the Sun. Such plasma processes are thought to be of fundamental importance all over the universe. Therefore the polar atmosphere is a natural laboratory in which physical processes can be studied.

The lowest part of the Earth's atmosphere is called the troposphere and it extends from the surface up to about 10 km. The atmosphere above 10 km is called the stratosphere, followed by the mesosphere. It is in the stratosphere that incoming solar radiation creates the ozone layer. At heights of above 80 km, in the thermosphere, the atmosphere is so thin that free electrons can exist for short periods of time before they are captured by a nearby positive ion. The number of these free electrons is sufficient to affect radio propagation coming both from inside and outside the globe. This portion of the atmosphere is ionized and contains a plasma which is referred to as the ionosphere.

2.1. The ionospheric layers and their production

The ionosphere is the uppermost part of the atmosphere, ionized by solar radiation (mainly by UV). The ionosphere can be considered as a variable shell of plasma surrounding the earth. It has an important role in atmospheric electricity and forms the inner edge of the magnetosphere. It has practical importance because, among other functions, it influences the incident radio noise from extraterrestrial sources and also radio propagation to distant places on the Earth. Ionosphere is located in the Thermosphere. Typically there is a maximum in the electron density profile at around 300 km (Fig. 2.1). The secondary peak at around 100km can grow larger and lower like during auroral activities.

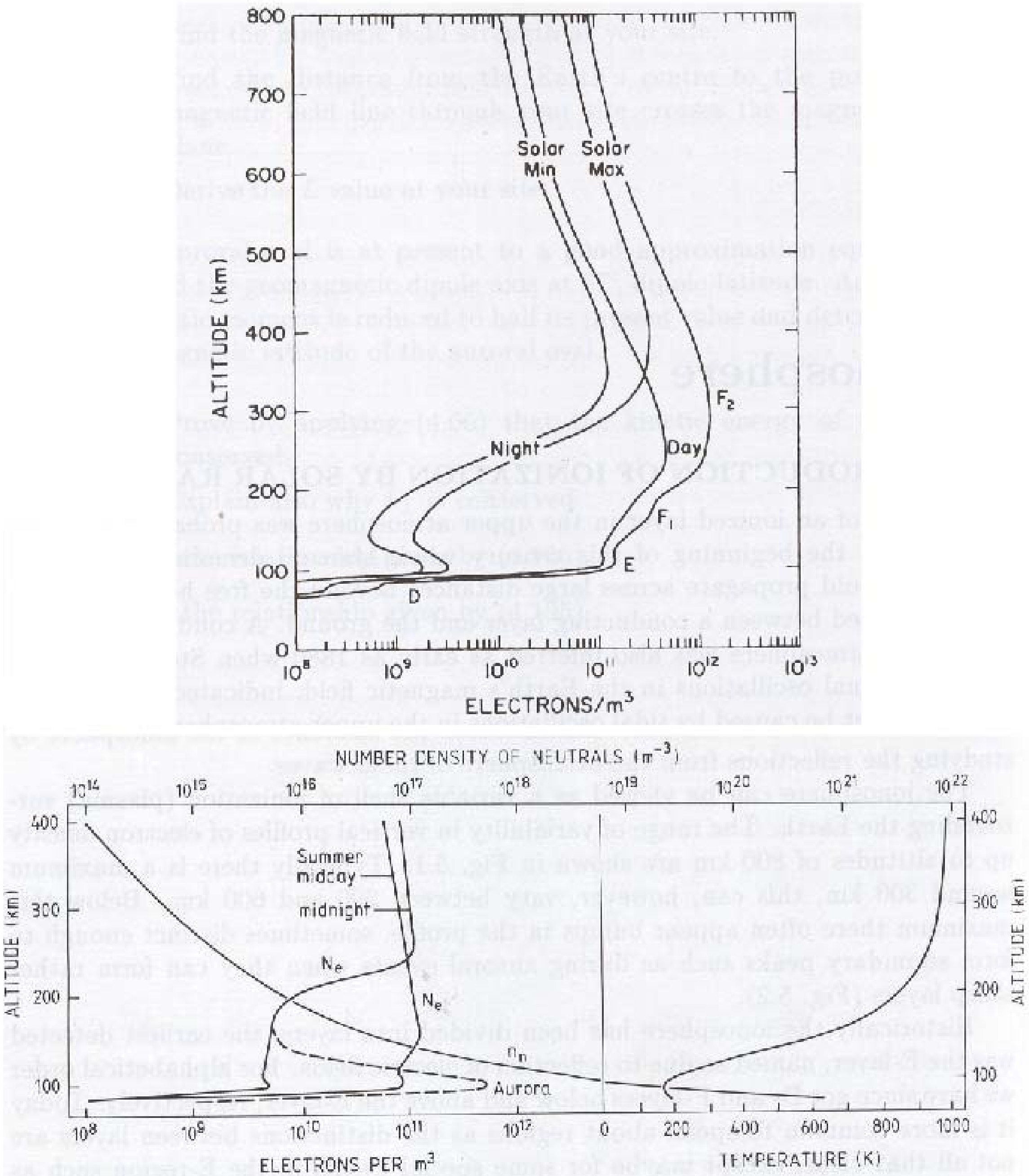

Fig. 2.1. Upper panel: Typical Electron density profiles for sunspot max. and min. conditions; Lower Panel: Electron density profiles and a secondary Auroral peak in it. Neutral density and Atmosphere Temperature profiles are also shown [Brekke, 1997]

Solar radiation at ultraviolet (UV) and shorter X Ray wavelengths is considered to be ionizing since photons at these frequencies are capable of dislodging an electron from a neutral gas atom or molecule during a collision. At the same time, however, an opposing process called recombination begins to take place in which a free electron is "captured" by a positive ion if it moves close enough to it. As the gas density increases at lower altitudes, the recombination process accelerates since the gas molecules and ions are closer together. The point of balance between these two processes determines the degree of ionization present at any given time/ height.

Solar radiation, acting on the different compositions of the atmosphere with height, generates layers of ionization. The E_layer was detected earliest and named so due to reflection of *electric* fields. The lower and upper layers were named for alphabetical order respectively. Today, it is more common to speak about *regions*, since the borders in between are not that clear [Brekke 1997].

The ionization profile of the upper atmosphere

The degree of ionization in the ionosphere depends primarily on the Sun and its activity. There is a diurnal effect and a seasonal effect too. The local winter hemisphere is tipped away from the Sun, thus there is less received solar radiation. The activity of the sun is associated with the sunspot cycle, with more radiation occurring with more sunspots. Radiation received also varies with geographical location (polar, auroral zones, mid-latitudes, and equatorial regions). There are also mechanisms that disturb the ionosphere, disturbances such as solar flares and the associated release of charged particles into the solar wind which reaches the Earth and interacts with its geomagnetic field.

For a horizontal stratified static atmosphere in hydrostatic equillibrium, assuming that the gases in the atmosphere are ideal gases, the Chapman equation gives the ion production rate at each height:

$q= q_{m,0} \exp(1-x-\sec\chi \exp(-x))$ (2.1)

Where:

q is the ion production rate at height z,

the 0 index stands for zero zenith angle and the *m* index symbolizes the term maximum,

H is the scale height of the atmosphere,

χ is the zenith angle of solar irradiation,

$x=(z-z_{m0})/H$ is the normalized height reduced to the height of maximum ionization for overhead sun,

χ is the zenith angle of solar irradiation,

C is the ionization production efficiency (i.e. for every unit of incident energy absorbed in the path ds, there will be formed a number C electrons, so : $q=-CdI/ds$, note that we have: $dI=-n\sigma(\lambda)Ids$, and the absorption cross section, $\sigma(\lambda)$, depends on wavelength of the radiation.).

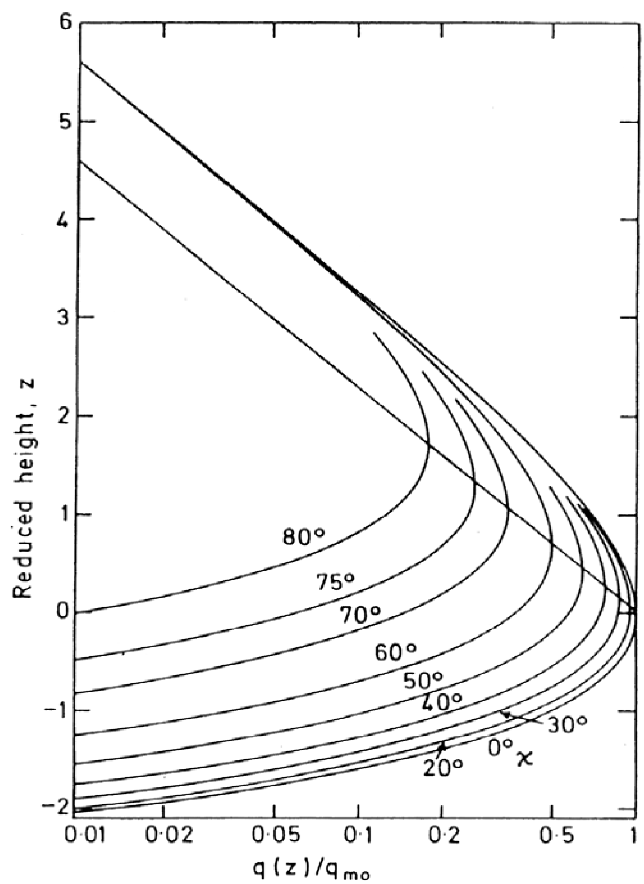

Fig. 2.2. Chapman production profiles for different solar zenith angles [Brekke 1997]

For a real target atmosphere and a real solar spectrum, the ion production profile calculation is a rather time consuming effort. The upper atmosphere is constructed of different gases with different scale heights, and the solar radiation spectrum consists of lines and bands with different intensities. Therefore, to calculate the ionization rates in different regions, a nutral atmospheric model is usually assumed, with height distribution of some of the the major gases in concern, and for a finite number of wavelengths the individual production profiles are derived (Fig. 2.3)

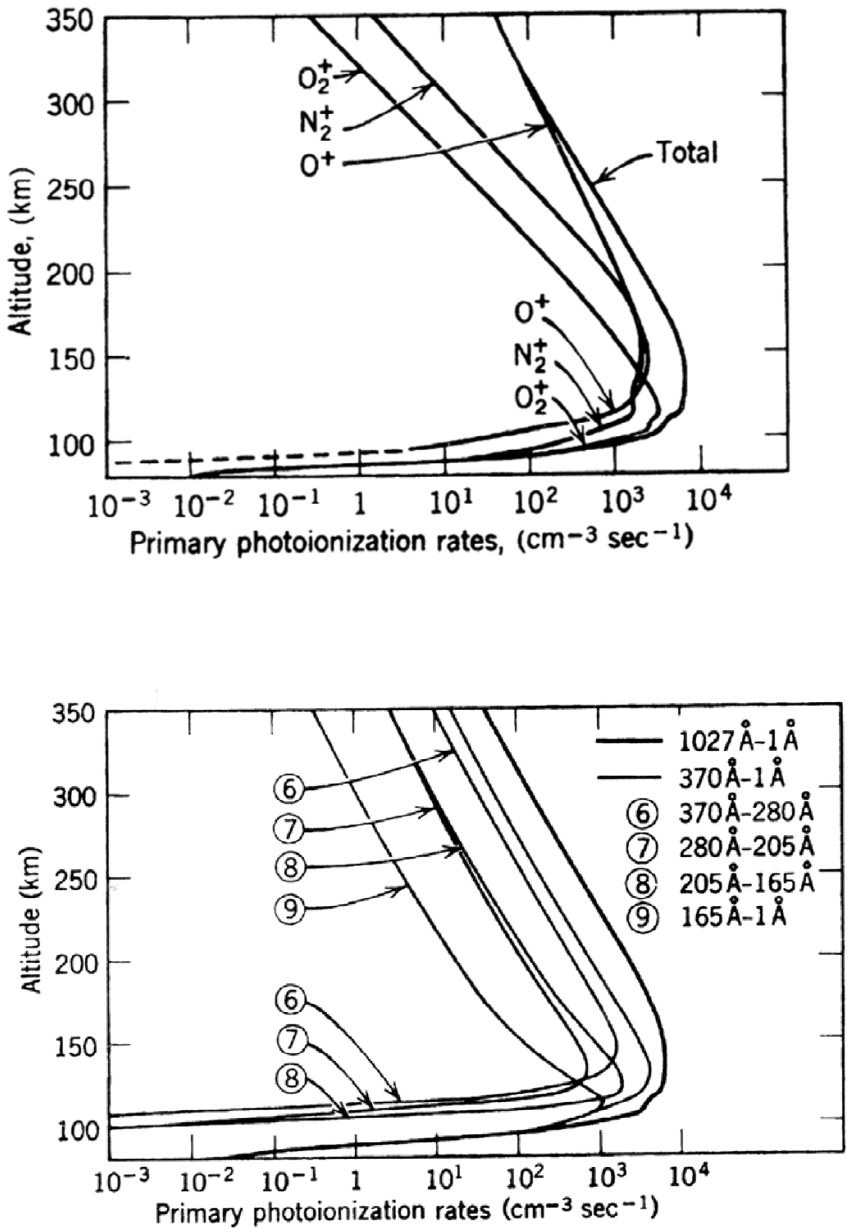

Fig. 2.3. Calculated ionization rates in the E and F regions [Brekke, 1997].

The recombination process

Neglecting the transport of ions, and assuming that the electrons are caught only by ions, the ion loss rate,l_i, in photochemical equillibrium will be proportional to the product of electron density and ion density, with a factor of recombination coefficient, α:

$l_i=\alpha\ n_e\ n_i=\alpha\ n_e\ n_e=\alpha\ n_e^2$ (2.2)

and this loss rate will reach an equillibrium with the ion production rate($l_i=q_i$):

$q_{m,0}\ \exp(1-x-\sec\chi\ \exp(-x))=\alpha\ n_e^2$ (2.3)

Therefore, the electron density at any given height z is given by:

$n_e\ (z)=\sqrt{\frac{q_{m,0}}{\alpha}}\ \exp[\frac{1}{2}(1-x-\sec\chi\ \exp(-x))]$ (2.4)

By neglecting the height variations of the recombination coefficient, the electron density will have a maximum when exp(-x)=cosχ.

On the other hand, if the electrons are lost by attachment to a molecule, the loss rate will be proportional to the electron density:

$l_i=\beta\ n_e$ (2.5)

where, β is proportional to density of molecules, [M], and this loss rate will reach an equillibrium with the ion production rate($l_i=q_i$):

$q_{m,0}\ \exp(1-x-\sec\chi\ \exp(-x))=\beta\ n_e$ (2.6)

Therefore, the electron density at any given height z is given by:

$n_e\ (z)=\ q_{m,0}\ \exp[1-x-\sec\chi\ \exp(-x)]/\ \ \beta$ (2.7)

Similarly, by neglecting the height variations of β, the electron density will have a maximum when exp(-x)=cosχ.

The negative ions formed in the attachment process, are not so effective above E region, but important in the lower ionosphere [Brekke, 1997].

In relating proton flux (e.g. coming from Coronal Mass Ejections) to the electron density, the greatest uncertainty source is the α factor [Hargreaves and Birch 2005].

D layer

The D layer (D Region) is the innermost layer, 55 km to 90 km above the surface of the

Earth which has an electron density in the order of $10^2 - 10^4$ cm^{-3}. Ionization is due to Lyman series-alpha hydrogen radiation at a wavelength of 121.5 nanometre (nm) ionizing nitric oxide (NO). In addition, when the sun is active with 50 or more sunspots, hard X rays (wavelength < 1 nm) ionize the air (N_2, O_2). During the night cosmic rays produce a residual amount of ionization. Recombination is high in the D layer, thus the net ionization effect is very low. The frequency of collision between electrons and other particles in this region during the day is about 10 million collisions per second. The layer reduces greatly after sunset, but remains due to galactic cosmic rays. A common example of the D layer effect in action is the disappearance of distant AM broadcast band stations in the daytime. During solar proton events, ionization can reach unusually high levels in the D-region over the high and polar latitudes. Such events are known as Polar Cap Absorption (PCA) events, because the increased ionization significantly enhances the absorption of radio signals passing through the region. Such events typically last less than 24 to 48 hours. Fig. 2.4 shows the electron concentration profiles in the D region, during quiet and active sun.

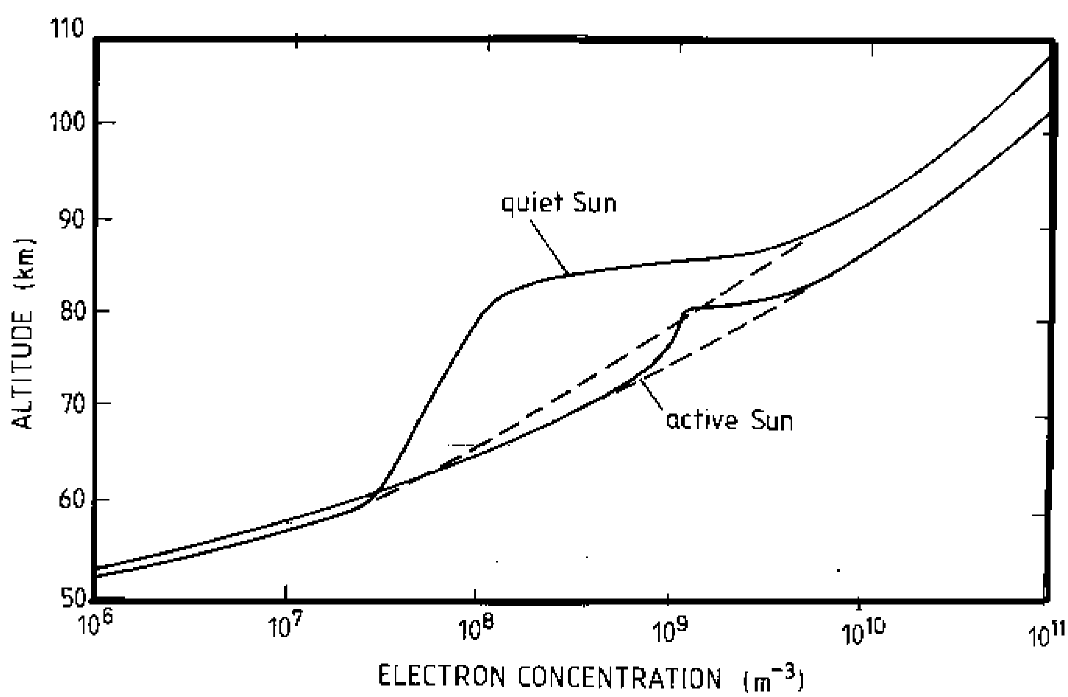

Fig. 2.4. Schematic electron concentration profiles in the D-Region for quiet and active solar conditions [Brekke 1997]

E layer

This region is also known as Kennelly-Heaviside layer or simply the Heaviside layer. Its existence was predicted in 1902 independently and almost simultaneously by the American electrical engineer Arthur Edwin Kennelly (1861-1939) and the British physicist Oliver Heaviside (1850-1925). However, it was not until 1924 that its existence was detected by Edward V. Appleton. The E layer is the middle layer of the ionosphere, 90 km to 120 km above the surface of the Earth. Ionization is due to soft X ray (1-10 nm) and far ultraviolet (UV) solar radiation ionization of molecular oxygen (O_2). Here, n_e is in the order of several 10^5 cm^{-3}.

The vertical structure of the E layer is primarily determined by the competing effects of ionization and recombination. At night the E layer begins to disappear because the primary source of ionization, the sun, is no longer present. This results in an increase in the height where the layer maximizes because recombination is faster in the lower layers. Diurnal changes in the high altitude neutral winds also plays a role. The increase in the height of the E layer maximum increases the range to which telecommunication radio waves can travel by reflection from the layer [Hargreaves 1979].

F layer

The F layer is 120 km to 400 km above the surface of the Earth. It is the top most layer of the ionosphere. In this region, n_e is in the order of several 10^6 cm^{-3}.

Here extreme ultraviolet (UV) (10-100 nm) solar radiation ionizes atomic oxygen (O). In terms of HF communications, the F region is the most important part of the ionosphere. The F layer divides into two layers, the F_1 and F_2 in the presence of sunlight (during daytime) and combines into one layer at night. The F layers are responsible for most skywave propagation of radio waves, and are thickest and most reflective of radio on the side of the Earth facing the sun [Hargreaves 1979].

2.2. Sources of ionization enhancement

2.2.1. Solar radiation and solar activity storms

Solar variations are changes in the amount of radiant energy emitted by the Sun. There are periodic components to these variations, the principal one being the 11-year solar cycle (or sunspot cycle), as well as aperiodic fluctuations. Solar activity has been measured via satellites during recent decades and through 'proxy' variables in prior times. Sunspots are relatively dark areas on the surface of the Sun where intense magnetic activity inhibits convection and so cools the surface. The number of sunspots correlates with the intensity of solar radiation. The variation is small (of the order of 1 W/m^2 or 0.1% of the total) and was only established once satellite measurements of solar variation became available in the 1980s.

Solar flares

A solar flare is a violent explosion in the solar corona and chromosphere, heating plasma to tens of millions of kelvins and accelerating electrons, protons and heavier ions to near the speed of light. They produce electromagnetic radiation across the electromagnetic spectrum at all wavelengths from long-wave radio to the shortest wavelength gamma rays. Most flares occur in active regions around sunspots, where intense magnetic fields emerge from the Sun's surface into the corona. Flares are powered by the sudden (timescales of minutes to tens of minutes) release of magnetic energy stored in the corona.

X rays and UV radiation emitted by solar flares can affect Earth's ionosphere and disrupt long-range radio communications. Solar flares were first observed on the Sun in 1859 as localized brightenings in a sunspot group. The frequency of occurrence of solar flares varies, from several per day when the Sun is particularly *"active"* to less than one each week when the Sun is *"quiet"*. Large flares are less frequent than smaller ones. At the peak of the cycle there are typically more sunspots on the Sun, and hence more solar flares.

Solar flares are classified as A, B, C, M or X according to the peak flux (in W/m^2) of 100 to 800 picometer X rays near Earth, as measured on the GOES spacecraft. Each class has a peak flux ten times greater than the preceding one, with X class flares having a peak flux of order 10^{-4} W/m^2. Within a class there is a linear scale from 1 to 9, so an X2 flare is twice as powerful as an X1 flare, and is four times more powerful than an M5 flare. The more powerful M and X class flares are often associated with a variety of effects on the near-Earth space environment. Although the GOES classification is commonly used to indicate the size of a flare, it is only one measure (Fig. 2.5).

Solar flares and associated Coronal Mass Ejections (CMEs) strongly influence our local space weather. They produce streams of highly energetic particles in the solar wind and the Earth's magnetosphere that can present radiation hazards to spacecraft and astronauts. The soft X ray flux of X class flares increases the ionisation of the upper atmosphere, which can interfere with short-wave radio communication, and can increase the drag on low orbiting satellites, leading to orbital decay.

Solar flares release a cascade of high energy particles known as a proton storm. Most proton storms take two or more hours from the time of visual detection to reach Earth. A solar flare on January 20, 2005 released the highest concentration of protons ever directly measured, taking only 15 minutes after observation to reach Earth, indicating a velocity of approximately one-third light speed. The radiation risk posed by solar flares and CMEs is one of the major concerns in discussions of manned missions to Mars or to the moon. Some kind of physical or magnetic shielding would be required to protect the astronauts. Originally it was thought that astronauts would have two hours time to get into shelter, but based on the January 20, 2005 event, they may have as little as 15 minutes to do so (http://www.spaceweather.com/).

Solar Proton Events (SPE)

A Solar proton event occurs when protons emitted by the Sun become accelerated to very high energies either close to the Sun during a solar flare or in interplanetary space by the shocks associated with coronal mass ejections. Arguments continue as to whether the acceleration is driven by the X ray flare release process or in solar wind shock fronts during coronal mass ejections [*Krucker and Lin*, 2000; *Cane et al.*, 2003]. Satellite data show that the protons involved have an energy range spanning 1 to 500 MeV, occur relatively infrequently, and show high variability in their intensity and duration [*Shea and Smart*, 1990]. These high energy protons can penetrate the Earth's magnetic field and cause ionization in the ionosphere. Solar protons normally have insufficient energy to penetrate through the Earth's magnetic field. However, during unusually strong solar flare events, protons can be produced with sufficient energies to penetrate deeper into the Earth's magnetosphere and ionosphere. The effect of the Solar Proton Events is confined to the polar cap regions, where the particles are guided by the magnetic field.

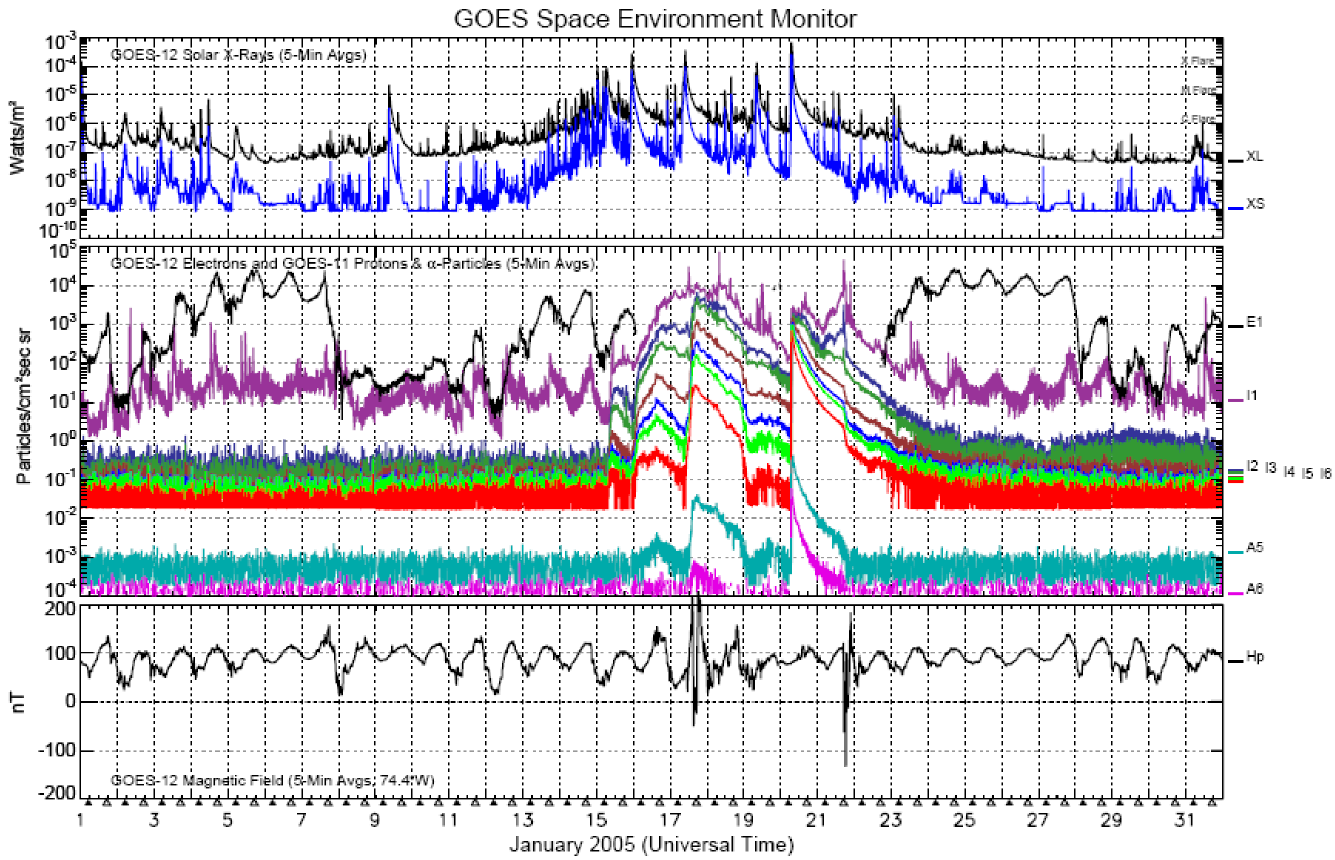

GOES SEM Data Key

- **XL** 1 - 8 Å X-rays (Watts/m^2)
- **XS** 0.5 - 3 Å X-rays, or 0.5 – 4 Å prior to GOES-8 (Watts/m^2)
- **E1** > 2 MeV (Electrons/cm^2 sec sr)
- **I1** > 1 MeV (Protons/cm^2 sec sr)
- **I2** > 5 MeV (Protons/cm^2 sec sr)
- **I3** > 10 MeV (Protons/cm^2 sec sr)
- **I4** > 30 MeV (Protons/cm^2 sec sr)
- **I5** > 50 MeV (Protons/cm^2 sec sr)
- **I6** > 60 MeV (Protons/cm^2 sec sr)
- **I7** > 100 MeV (Protons/cm^2 sec sr)
- **A5** 150-250 MeV, 160-260 prior to GOES-8 (α-particles/cm^2 sec sr MeV)
- **A6** 300-500 MeV, 330-500 prior to GOES-8 (α-particles/cm^2 sec sr MeV)
- H_P Perpendicular to orbital plane (nanotesla)
- H_E Earthward (nanotesla)
- H_N Normal to H_P and H_E,
- △ Satellite Local Noon
- ▲ Satellite Local Midnight

Fig. 2.5. A Summary plot of GOES satellite measurements in January 2005

(From http://goes.ngdc.noaa.gov/)

Ion chemistry leads to increased production of odd nitrogen ($NO_x = N + NO + NO_2$) and odd hydrogen ($HO_x = H + OH + HO_2$) which participate in catalytic reaction cycles that decrease the amount of ozone in middle atmosphere. HO_x gases have a short chemical lifetime but the NOx gases are mainly destroyed by photodissociation. Hence during winter, when little or no sunlight is available in the polar atmosphere, the effect of the NO_x cycles can be long-lasting [Seppälä et al. 2005].

X rays: sudden ionospheric disturbances (SID)

When the sun is active, strong solar flares can hit the Earth with hard X rays on the sunlit side of the Earth. They will penetrate to the D-region, release electrons which will rapidly increase absorption causing a High Frequency (3-30 MHz) radio blackout. As soon as the X rays end, the sudden ionospheric disturbance (SID) or radio black-out ends as the electrons in the D-region recombine rapidly and signal strengths return to normal.

Polar cap absorption (PCA)

PCA's are a direct consequence of energetic protons emitted in solar flares. An Important characteristic of the PCA's is their relative uniformity over the polar cap. [Hargreaves 2005] These particles can hit the Earth within 15 minutes to 2 hours of the solar flare. The protons spiral around and down the magnetic field lines of the Earth and penetrate into the atmosphere near the magnetic poles increasing the ionization of the D and E layers. PCA's typically last anywhere from about an hour to several days, with an average of around 24 to 36 hours.

Ground Level Enhancement (GLE)

GLE is an event in which the Sun produces energetic particles (Solar cosmic ray) of sufficient energy and intensity to increase radiation levels on the surface of the Earth. It is found that the solar cosmic rays vary widely in their intensity and spectrum, increasing in strength after some solar events such as solar flares. Further, an increase in the intensity of solar cosmic rays is followed by a decrease in all other cosmic rays, called the Forbush decrease after their discoverer, the physicist Scott Forbush. These decreases are due to the solar wind with its entrained magnetic field sweeping some of the galactic cosmic rays outwards, away from the Sun and Earth.

2.2.2. Geomagnetic activity and disturbances

Geomagnetic storms

Earth's magnetic field (and the surface magnetic field) functions approximately like a magnetic dipole, with one pole near the north pole (i.e. the Magnetic North Pole) and the other near the geographic south pole (the Magnetic South Pole). An imaginary line joining the magnetic poles would be inclined by approximately 11.2° from the planet's axis of rotation. It is probably fair to claim that no existing theory about the source of this magnetic field can explain all its history. The cause of the field is probably explained by dynamo theory. Magnetic fields extend infinitely, though they are weaker farther from their source. The strength of the field at the Earth's surface ranges from less than 30 microteslas (0.3 gauss) in an area including most of South America and South Africa to over 60 microteslas (0.6 gauss) around the magnetic poles in northern Canada and south of Australia, and in part of Siberia. The field is similar to that of a bar magnet, but this similarity is superficial. The magnetic field of a bar magnet, or any other type of permanent magnet, is created by the coordinated spins of electrons and nuclei within iron atoms. The Earth's core, however, is hotter than 1043 K, the Curie point temperature at which the orientations of spins within iron become randomized. Such randomization causes the substance to lose its magnetic field. Therefore the Earth's magnetic field is caused not by magnetized iron deposits, but mostly by electric currents in the liquid outer core. [Hollenbach, D. F.; J. M. Herndon (2001), Herndon, J. M. (2003)]

Using magnetic instruments and magnetometers adapted from airborne magnetic anomaly detectors developed during world war II to detect submarines, the magnetic variations across the ocean floor have been mapped. The basalt — the iron-rich, volcanic rock making up the ocean floor — contains a strongly magnetic mineral (magnetite) and can locally distort compass readings. The pressure balance between the solar wind and the geomagnetic field is delicate, and perturbations in solar-wind velocity can cause the magnetosphere to oscillate, especially when the Sun emits a sudden gust of solar wind, a so-called coronal mass ejection. If this impacts upon the magnetosphere then a magnetic storm can follow. Alternatively, magnetic storms can also be caused by a process called 'magnetic reconnection'; A highly dynamic process, which causes the magnetic field measured at the Earth's surface to become extremely active.

Frequently, the Earth's magnetosphere is hit by solar flares causing geomagnetic storms. A geomagnetic storm is a temporary intense disturbance of the Earth's magnetosphere. During a geomagnetic storm the F_2 layer will become unstable, fragment, and may even disappear completely. In the Northern and Southern pole regions of the Earth aurora will be observable in the sky (Fig.2.6 presents an overall view of this process).

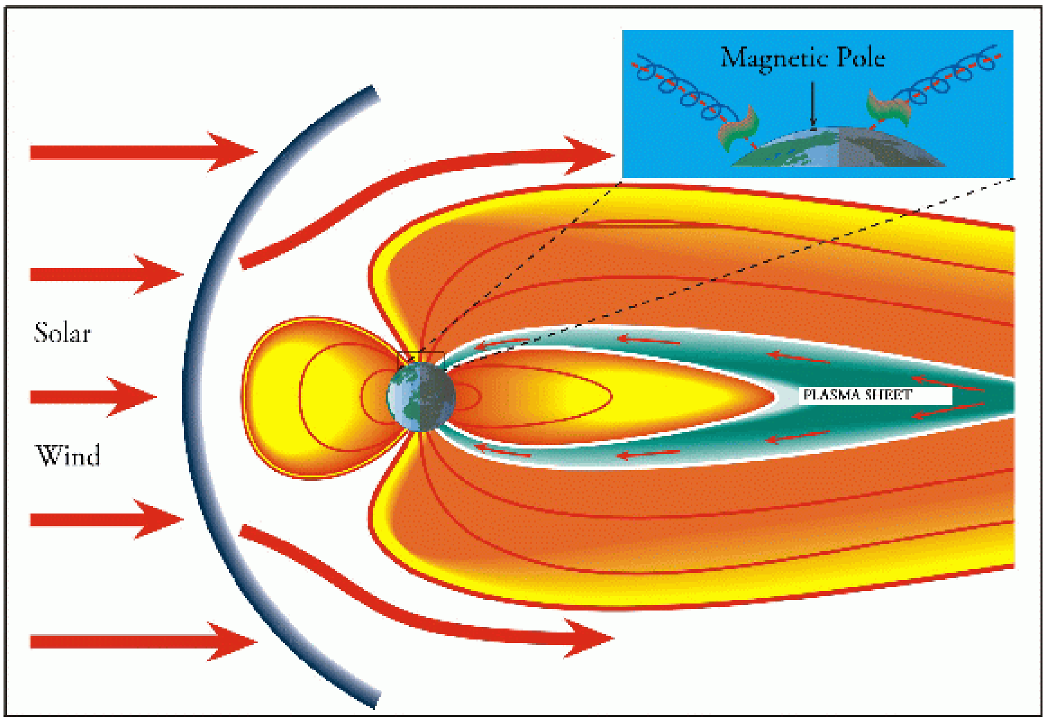

Fig. 2.6.The Earth's magnetosphere against solar wind /flares causing geomagnetic storms. The magnified inset shows the incoming electrons spiraling down magnetic field lines may energize the atmospheric gases to emit light (http://www.dcs.lancs.ac.uk/iono/).

For more than a century, magnetic observations from ground at high latitude have been used to deduce the so-called equivalent current system. After great developments by Birkeland and Harang, Silsbee and Vestine (1942) depicted the Horizontal Magnetic Field fluctuations and the corresponding contour lines of constant current densities. Fig. 2.7 depicts such ionospheric electric currents.

Fig. 2.7. Ionospheric Electric Currents. Schematic diagram of the electric-current pattern in the ionosphere driven by diurnal heating from the Sun. Note that the current is concentrated on the day side, consisting of two oppositely oriented circuits (http://geomag.usgs.gov)

The short-term instability of the magnetic field is measured with the ***K-index.*** The K-index quantifies disturbances in the horizontal component of earth's magnetic field with an integer in the range 0-9 with 1 being calm and 5 or more indicating a geomagnetic storm. It is derived from the maximum fluctuations of horizontal components observed on a magnetometer during a three-hour interval. The conversion table from maximum fluctuation (nT) to K-index, varies from observatory to observatory in such a way that the historical rate of occurrence of certain levels of K are about the same at all observatories. In practice this means that observatories at higher geomagnetic latitude require higher levels of fluctuation for a given K-index. The real-time K-index is determined after the end of prescribed three hourly intervals (00:00-03:00, 03:00-06:00, ..., 21:00-24:00). The maximum positive and negative deviations during the 3-hour period are added together to determine the total maximum fluctuation. These maximum deviations may occur any time during the 3-hour period (http://www.swpc.noaa.gov/info/Kindex.html).

3. Cosmic radio noise and its measurement

The natural extraterrestrial cosmic radio noise power is continuously incident on the earth's atmosphere. Cosmic Noise (Ionospheric) Absorption (CNA) is a reliable indicator of excess-Absorption Events occurring especially at high latitudes under disturbed conditions (solar flares/X rays, coronal mass ejections/solar proton events, geomagnetic storms/precipitating high energetic particles). However, the accuracy in determination of normal absorption depends critically on the short-term and long-term stability of receiver gain. All units of the receiving system have to be stabilized by using electronically stabilized power supplies, local oscillators, temperature stabilization of the equipment, and avoiding transmission losses between antenna and receiver.

3.1. Extra-terrestrial sources of radio noise

In the upper HF and lower VHF bands the major contribution to the cosmic noise comes from our own galaxy. Smaller contributions are due to the more intense discrete sources of both galactic and extragalactic origin and to the sun. Radio noise from the Sun at wavelengths around 10m can normally be neglected, since the undisturbed noise power from the sun is less than one percent of the noise power from the diffuse background observed on a wide beam antenna. But when the sunspot groups are present and at times of solar flares and similar events, the sun's radio output can even dominate the total noise received [Rawer, 1976].

A source of variations in received power is the *scintillation of discrete extraterrestrial radio sources* due to diffraction effects in the ionosphere. These scintillations take the form of variations (period of about 30 s) in the intensity of the localised sources such as the Cygnus or Cassiopeia. Ionospheric scintillation is due to irregularities in the ionosphere being illuminated by the strong point source. The irregularities act like a diffraction grating and the receiver measures large variations in signal strength, depending on whether the wave fronts are constructive or cancelling out. These variations average out in case of wide beam antenna and also if the time resolution of the system is higher than about 2 minutes [Rawer, 1976].

The intensity of *the radio noise originating in the ionosphere* will normally be very small compared with that of extra-terrestrial radio sources [Rawer, 1976].

It is usual to use the *equivalent temperature, T,* concept in discussing (Cosmic Radio) noise power, $P=kTB$, where k is the Boltzman's constant and B is the effective bandwidth. The equivalent temperature of the galaxy (i.e. the main source of the Cosmic Noise power) is a strong function of frequency, varying approximately as $f^{-\psi}$ where ψ is the spectral index. For example the equivalent temperature of the galaxy is about 30000K at 30 MHz and about 200K at 200 MHz [Rawer, 1976, Campistron 2001]. The spectral index can be assumed to be constant over a frequency band; it is around 2.5 between 38 and 404 MHz [Campistron et al. 2001].

3.1.1 Ionospheric radio wave absorption and its mechanism

The (geo)magnetic rigidity (defined as the momentum per unit charge m.v/q) is usually used as a measure for the ability of particles to penetrate a specific magnetic field [Brekke 1997], i.e. there is a minimum rigidity needed for a particle to penetrate to a given geomagnetic latitude (i.e. higher rigidity is needed to penetrate at a lower latitude). Therefore, every geomagnetic position has a corresponding cutoff rigidity. In general the geomagnetic cutoff rigidity of a particle is also a function of its direction of arrival [Rodger et al. 2006]. While this effect was initially modeled with a static dipole field, the geomagnetic cutoff rigidity is a much more dynamic quantity depending on the Earth's internal and external magnetic fields. As such the geomagnetic cutoff varies spatially and with time, on timescales of both the internal (years) [*Smart and Shea*, 2003] and the external field (minutes-hours) [*Kress et al.*, 2004]. Charged particles from solar flares, penetrate and ionize the polar atmosphere to altitudes typically ranging from 30 to 120 km depending on their type and energy [Rosenberg, 1991]. As a consequence of the enhanced electron density in the region, the Cosmic Radio Noise at HF and VHF frequencies is attenuated compared to the signal that would pass through an undisturbed ***quiet*** ionosphere. It has been shown that there is an empirical relationship between the square root of the integral proton flux (>10 MeV) and cosmic noise absorption in daytime, at least when geomagnetic rigidity cutoff effects do not limit the fluxes [*Kavanagh et al.*, 2004]. Fig. 3.1. shows the fluctuations in cut off geomagnetic rigidity at different latitudes during a solar activity period in January 2005.

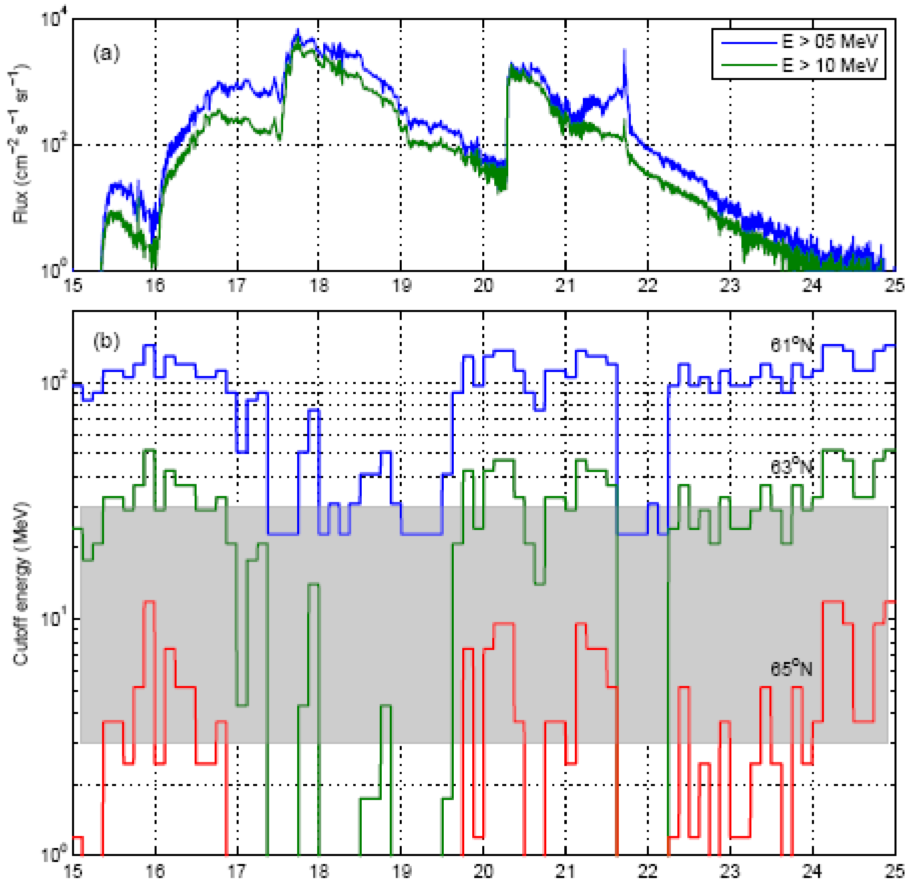

Fig. 3.1. (a) Proton fluxes measured at Geostationary Orbit by the GOES-11 satellite during January 15-25, 2005 (b) Estimated cutoff energies at selected magnetic latitudes. The grey area indicates the approximative energy range of protons depositing their energy in the mesosphere, i.e. 3–30MeV [Veronen et al. 2005]

Measuring ionospheric absorption is indeed measuring the attenuation by loss of energy or transfer of energy from the (radio) wave into the medium. When reducing measured data, attenuation caused by other than this energy transfer must be eliminated as much as possible. Absolute field measurements demand antennas whose absolute characteristics are accurately known and can be misleading due to environmental influences which are not easy to avoid. Therefore, most measurements are based upon relative field strength, comparing radio frequency voltages in the receiver instead of absolute measurements of the fields outside. The only condition is that the factors which determine the effective gain must be kept constant.

An electromagnetic wave propagating through a plasma is refracted and in general, attenuated as a consequence of forced oscillations of the electrons due to the alternating electric field of the wave. The effects depend on the amplitude and frequency of the wave: the lower the frequency, the greater the amplitude of the forced oscillations. The energy of the wave is partially transferred to these oscillations; per unit path, the energy transfer is proportional to the electron density in the plasma. The energy balance of the wave is not seriously changed, because an overwhelming part of the transferred energy is restored to the wave by secondary radiation of the electrons. Each oscillating electron acts like a secondary transmitter radiating on the same frequency as the wave. But the relevant secondary fields are shifted in phase relative to the original wave field. The transfer of energy from the wave and back to it is lossless provided that the electron does not suffer a collision with another particle; these collisions lead to irreversible attenuation of the wave.

Since the attenuation is produced by the collisions involving the oscillating electrons, it necessarily depends on two factors:

1) the efficiency of energy transfer from the wave into electron oscillations
2) the probability of collisions between electrons and other particles

The first one is concerned with the *source* of the energy loss and depends on the energy taken by electrons from the wave. This first factor is usually shown by a *dispersive factor.*

The mechanism is rather complicated in our ionosphere because of the presence of the Earth's magnetic field, which produces a kind of resonance effect at gyro frequency, f_L, (around the magnetic field line) for one of the two possible circular polarizations of the wave: namely for that for which the sense of rotation is the same as that of the natural free motion of the electrons in the field. The rotation frequency, f_L, is roughly 1 MHz at the earths surface, it varies with geomagnetic location of the station.

The second factor describes the true, loss mechanism, i.e. the collisions. The averaged effective collision frequency, ν, is usually used to show this factor. The collisional loss is then proportional to *νN*, where N is the electron density.

The absorption coefficient should therefore be obtained by a product of the dispersive factor and the *νN.*

Taking into account the influence of magnetic field and of collisions, the conditions of radio wave propagation in a plasma must be described by a rather complicated equation, the dispersion formula, first given by Lassen (1927), and by Sen and Wyller (1960) [Rawer, 1976].

The attenuation can be described by an exponential decrease of the field strength, E, of the wave, $E=E_0 \exp(-\int\kappa\, ds)$, where s is the path length and κ is the *absorption coefficient;* i.e.

$$\kappa = \frac{q^2}{2\varepsilon_0 m_e c_0 \mu} \cdot \frac{N\nu}{(\omega \pm \omega_L)^2 + \nu^2} \ .$$

N is the electron density, ν is the electron-neutral collision frequency, ω_L is the gyration frequency in direction of the propagation, q and m_e are the charge and the mass of the electron, c_0 is the speed of light in free space, $\omega = 2\pi f$ is the angular frequency of the radio wave and μ is the refractive index of the medium [Rawer, 1976].

The depth to which an incoming electron penetrates into the atmosphere depends on its initial energy (Rees, 1963), the more energetic ones depositing their energy at lower altitudes. The resulting electron-density profile, therefore, depends on the original spectrum of the incident particles. At any height, h , if the electron density is $N(h)$, the absorption of a radio wave of angular frequency $\omega = 2\pi f$ is $A_{dB} = 4.6 \times 10^{-5} \int \frac{N(h)\nu(h)}{\omega^2 + \nu^2} dh$ for f>30 MHz [Hargreaves, 1969].

While $\nu(h)$ is a property of the atmosphere (i.e. proportional to pressure), $N(h)$ depends on the incoming electron flux over a band of energies and thus, also on the particle energy. [Hargreaves, and Friedrich 2003].

Cosmic noise absorption should vary as a function of the radio frequency, $A(f) \sim f^{-2}$ at altitudes where ν is much less than the angular frequency of the radio wave, $2\pi f$, typically above ~70 km [Rosenberg and Detrick 1991, Sen and Wyller (1960)]. The spectral index is studied in a lot of experiments and during different phenomena, i.e. Auroral Absorptions, Polar Cap Absorptions, etc. It is estimated to be somewhere between 1.3 and 2.7 depending on the cause event and the model assumed for the absorbing region [Campistron et al. 2001].

3.2 The riometer experiment

Observed cosmic noise varies according to the earth's rotation, but remains constant for a repeated Local Sidereal Time. (For a description of sidereal time, see chapter 3.2.1. or [Duffet-Smith, 2003]). The cosmic noise power incident from a given direction in space, as measured with a fixed receiving system on the earth at a given sidereal time, ought to be constant if there were no absorption in the Earth's atmosphere. Consequently, the strength of cosmic noise actually measured at the surface of the Earth ought to be a reliable indicator of the integrated absorption produced by the intervening ionosphere. This fact was first realised by Shain in 1951 in Australia and the temporal variation in absorption was studied also by Mitra and Shain in 1953 using this idea at a frequency of 18.3 MHz. Since then, usefulness of the method has been greatly increased by employing servo-comparison and other techniques as embodied in riometers [Rawer, 1976].

The riometer (Relative Ionospheric Opacity Meter for Extra-Terrestrial Electromagnetic Radiation) was developed in the 1950s. Simple receiving systems had difficulties like Gain stabilization, calibration and power supply stabilization. (Hereafter, Cosmic Noise Absorption and Power, will be called CNA and CNP respectively.) Since the introduction of riometers, CNA is measured normally by riometers especially in the polar regions. The essential feature of riometer is a servo control unit that continuously compares the noise received from the antenna with the noise generated by a local noise diode and adjusts the latter to maintain the equality. Therefore the variations in the gain will affect both noise signals equally and thus only have the second-order effect of changing the amplitude of the "error" signal. Calibration is carried out by replacing the antenna by a second local noise generator whose output can be adjusted either manually or automatically to certain pre-set levels. The servo noise source will track these known input signals, producing a calibrated response that can be used to reduce the varying signal recorded by the antenna to actual power levels [Rawer, 1976].

Local interference from man-made "technical" noise (power lines, electrical machinery,...) may exist but can be largely avoided by choosing an appropriate site. Some riometers use a sweep frequency receiver (with a sweep of a few hundred Hz) combined with a Minimum Signal Detection.

Riometers were developed to avoid the problems of receiver gain stability. A riometer is a passive radio wave system inspired by radio astronomy techniques [G. Dekoulis, F. Honary, 2004] which require a low noise, high dynamic range, a Minimum Detectable

Signal (MDS) value as low as possible, and an auto-calibrated receiver to measure the background cosmic noise received by earth or another planet [G. Dekoulis, F. Honary, 2004]. A vertical antenna with the main lobe in the direction of local zenith can detect these cosmic radio signals.

The choice of riometer operating frequency is restricted by practical considerations. As the absorption is higher for the lower frequencies, the frequency should be as low as possible to detect the effect of weak ionisation. An absolute lower (frequency) limit is set by the highest critical frequency of the ionosphere. (The critical frequency is the limiting frequency at or below which a radio wave is refracted by an ionospheric layer at vertical incidence. It is proportional to the square root of electron density of the layer.) Even high above this limit, operation suffers from propagated interference. Experience has shown that above 30 MHz, these effects are normally reduced [Rawer, 1976]. Typical operating frequencies of riometers are 27.6, 29.7, 29.9, 30, 32, 32.4, 35, 38.2 and 51.4 MHz [G. Dekoulis, F. Honary, 2004] (i.e. 20 to 55 MHz). At these high frequencies, the signal is little affected even by large electron densities; therefore, this kind of ionospheric measurement is usually made at locations where very large additional ionization can be expected, i.e. notably in the auroral zone. Alternatively, this type of ionospheric absorption measurement is called A2 in contrast to A1, which is the observation of the signal strength of a vertically emitted HF burst (essentially an ionosonde with amplitude recording), or A3 which is the observation of a distant transmitter at a fixed frequency. Both methods A1 and A3 depend on the reflection by the ionosphere, hence the received signal strength is also a function of the (a priori unknown) height of the reflection layer [Friedrich et al. 2001].

The absorption suffered by a radio wave in traversing the ionosphere is usually expressed in decibels (dB) and is found from the expression:

$A=10 \log(p/p_0)$ (3.1)

$A_{dB}= P_0-P$ (3.2)

Where P_0 is the non-attenuated CNP, and P is the CNP attenuated by atmospheric (Ionospheric) absorption, both measured at the same sidereal time (i.e. the same view angle to the sky). (Also $P=10 \log p$, $P_0=10 \log p_0$)

To measure the absorption, at first P_0 (i.e. the Quiet Day Curve) has to be estimated.

Riometers can be categorized into two major groups:

a. Imaging Riometer, consisting of an Array of antennae forming Multiple Narrow Beams
b. (Single) Wide beam Riometers (older systems)

Before getting into the details of practical implementation of the above equations, the concept of sidereal time needs to be illustrated.

3.2.1. Sidereal time

Universal time and the local civil time are relative to the motion of the Sun. In contrast, Sidereal time is a measure of the position of the Earth in its rotation around its axis, or time measured by the apparent diurnal motion of the vernal equinox, which is very close to, but not identical to, the motion of stars. Sidereal time is defined as the hour angle of the vernal equinox. When the meridian of the vernal equinox is directly overhead, local sidereal time is 00:00. Greenwich Sidereal Time is the hour angle of the vernal equinox at the prime meridian at Greenwich, England; local values differ according to longitude. When one moves eastward 15° in longitude, sidereal time is larger by one hour.
Sidereal time is used at astronomical observatories because it makes it very easy to work out which astronomical objects will be observable at a given time. Objects are located in the night sky using right ascension and declination relative to the celestial equator (analogous to longitude and latitude on Earth), and when sidereal time is equal to an object's right ascension, the object will be at its highest point in the sky, at which time it is best placed for observation, as atmospheric extinction is minimised.

Solar time is measured by the apparent diurnal motion of the sun, and local noon in solar time is defined as the moment when the sun is at its highest point in the sky (exactly due south or north depending on the observer's latitude and the season). The average time taken for the sun to return to its highest point is 24 hours.

During the time needed by the Earth to complete a rotation around its axis (a sidereal day), the Earth moves a short distance (around 1°) along its orbit around the sun. Therefore, after a sidereal day, the Earth still needs to rotate a small extra angular distance before the sun reaches its highest point. A solar day is, therefore, around 4 minutes longer than a sidereal day. The stars, however, are so far away that the Earth's movement along its orbit makes a generally negligible difference to their apparent direction and so they return to their highest point in a sidereal day (Fig. 3.2.). Another way to see this difference is to notice that, relative to the stars, the Sun appears to move around the Earth once per year. Therefore, there is one less solar day per year than there are sidereal days. This makes a sidereal day approximately $^{365.24}/_{366.24}$ times the length of the 24-hour solar day, giving approximately 23 hours, 56 minutes, 4.1 seconds (86,164.1 seconds).

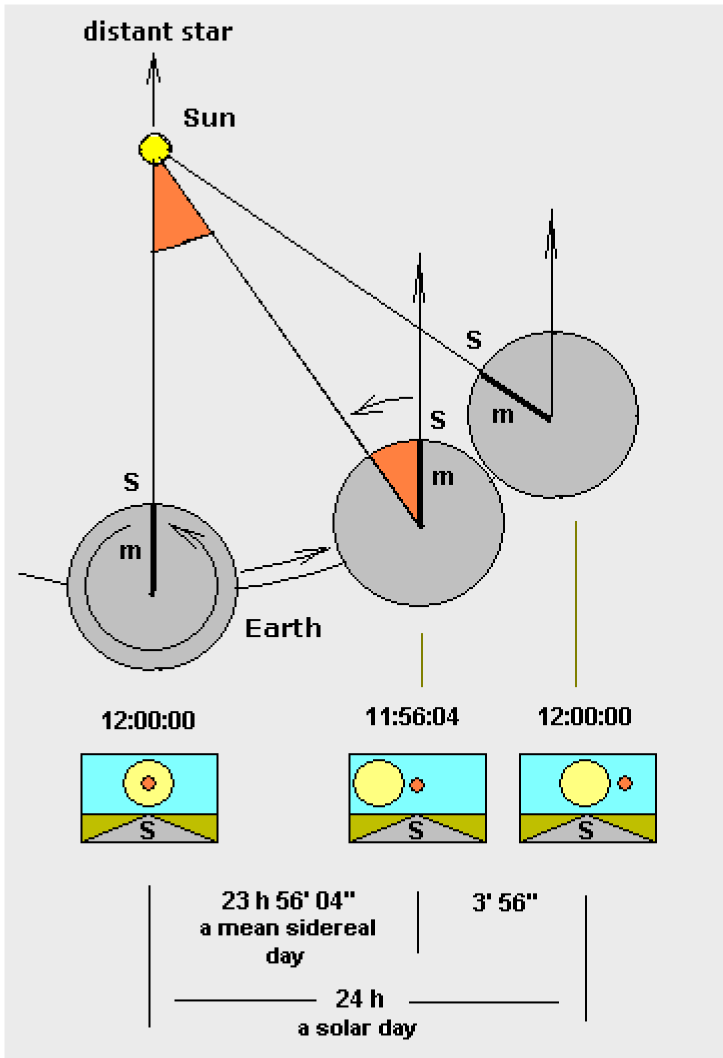

Fig. 3.2. Sidereal time vs solar time: Above left: a distant star (the small red circle) and the Sun are at culmination, on the local meridian. *Centre*: only the distant star is at culmination (a mean sidereal day). *Right*: few minutes later the Sun is on the local meridian again. A solar day is complete (http://en.wikipedia.org/).

3.2.2. Estimation of the Quiet Day Curve

The CNA depends on the ionisation in the ionosphere, and ionization depends primarily on the Sun and its activity. More ionization results in more absorption. Therefore, the received CNP is maximum at ***Quiet*** Solar/ Geomagnetic conditions (i.e. no Excess Ionisation). The high latitude ionosphere is more often disturbed than quiet [Harrich et al. 2003]. The determination of ionospheric absorption, CNA, as defined by equation (3.1) from cosmic noise power, measured at a given place and time with a fixed receiving system, requires the knowledge of the reference value, P_0, which should be recorded at the same place and time with the same receiving system in the absence of ionospheric absorption. Since the antenna beam, directed upward, each day explores the same strip of the sky according to the earth's rotation, this reference value (or curve) , P_0, will be a function of sidereal time. This means the unattenuated cosmic noise pattern repeats at intervals of one sidereal day, and thus the sidereal time ought to be used as the time base for the calculation of the CNA. This in combination with (3.2) means that:

$$CNA\ (t) = CNP(\text{no Absorption}) - CNP(t) \qquad (3.3)$$

$$= QDC - CNP(t) \qquad (3.4)$$

where the QDC is the so-called *Quiet Day Curve* measured at the Quiet conditions and both QDC and CNP(t) curves are plotted in sidereal time.

Quiet Day Curves are an indication of the noise level the device would be expected to measure on a day without any absorption, scintillation or interference. They can be generated by theoretical or empirical methods.

The first and most important step in CNA estimation/measurement is the preparation of the QDC as "the best possible estimate of the reference level, P_0, as a function of sidereal time." Manual preparation with great care and judgement by the scientists themselves is preferable to a pure mechanical procedure [Rawer, 1976].

For constructing the QDC, the basic assumption is that for any given sidereal time there is a certain part of the year in which the absorption becomes negligible. Consequently, the QDC is usually produced from a mass plot of individual readings of the output level (data points) as a function of sidereal time for a period during which there is no reason to suspect any changes in the equipment parameters. The upper envelope of this plot, or alternatively a curve that lies above 90 percent of the individual values, can be taken as the QDC. The highest actual value in each sidereal time (ST) interval (time bin) is considered to be a point of the QDC (namely a Quiet Day Point, QDP, shown above by P_0).

The reliability of the QDC can be improved by a careful selection of days with minimum interference, magnetically and ionospherically quiet conditions, equipment stability, etc.

After removing the data of non-quiet conditions the curve has to be estimated as maximum values in the time-bins of data. Most of the methods essentially involve studying the distribution of (cosmic noise signal) power levels measured in a given sidereal time interval over a period of many days. The size of the sidereal time interval (time resolution) depends on the amount of available data, and hence on the time resolution of the instrument (riometer,...) and the duration of the observation. Each time bin needs enough number of data points to be statistically analysed to provide a QDP with enough reliability.

Current Quiet Day Curve (QDC) estimation algorithms include the following:

A. Theoretical method, using data from a star survey

B. Empirical methods which include the following methods:

B.1. Percentile method: for each sidereal time (ST) interval, to estimate the corresponding QDP, this method takes the value higher than a specific percent (say 90%) of power values recorded in that ST interval. Normally a percentile between 80% to 95% is used. i.e. in this method the QDC is the curve which separates the highest (say) 10% of data points in the sidereal distribution from the remaining lower 90%.

B.2. Inflection point method: to estimate the corresponding QDP for each sidereal time interval, this method takes the higher inflection point of the distribution of the measured CNP values. Armstrong et al. [1977] proposed that instead of using an arbitrary percentage value for a given sidereal time interval, the value corresponding to the inflection point on the high-signal side of the peak of the distribution of cosmic noise levels in the interval should be used. This method seems to yield more acceptable QDCs for data with a moderate to high level of interference than the percentile method; but it demands a higher number of data available in each time bin (interval) [Drevin and Stoker, 1990].

B.3. Fourier transform/series method: A method for the determination of riometer quiet day curves which is based on the filtering of a discrete two-dimensional function or matrix. The two dimensions of the matrix are sidereal time and day number, with each row of the matrix representing one sidereal day. The filtering is done in the Fourier domain using a low-pass filter. With a low-pass filter the low frequency Fourier coefficients are retained, while the high frequency Fourier coefficients are discarded. The highest Fourier coefficient that is retained is the cutoff frequency of the filter [Drevin and Stoker, 1990].

Selection of the QDC estimation method depends mainly on the amount of available data (points). Generally, when the number of available data points is low, QDC estimation is pushed towards using the percentile method.

3.3. The narrow beam riometers IRIS and AIRIS

Before 1990, riometers generally operated with a broad beam antenna (60 degree full, -3 dB beam width), with a circular beam directivity (directional gain) pattern, although even from the earliest days narrow beam antennas have been used [Detrick and Rosenberg, 1990]. In practice, the antennas used are of the Yagi type. Depending on the actual shape of the antenna pattern, the single antenna (wide beam) biometer will receive HF power as a function of sidereal time [Friedrich et al. 2001]. Auroral absorption levels of 1 dB or more are common, as measured with broad beam antenna systems, while narrow beam values may be higher, due to (say) electron precipitation which does not cover the whole field of view of the wide beam antenna [Detrick and Rosenberg, 1990].

The wide beam riometers discussed above are simpler and more common, but pose problems which do not occur in imaging riometers with their narrow beams [Friedrich et al. 2001].

An imaging riometer has several beams not only in zenith, but also in some angular interval. It measures the absorption by using an array of antennas forming multiple narrow beams each looking at one portion of the total field of view. All the measurements (of all beams) together can be displayed in an image showing the current absorption not only in one point of the celestial sphere but in a whole region, for example inside a region of 200 × 200 km e.g. at 90 km height (Figs. 3.3, 3.4).

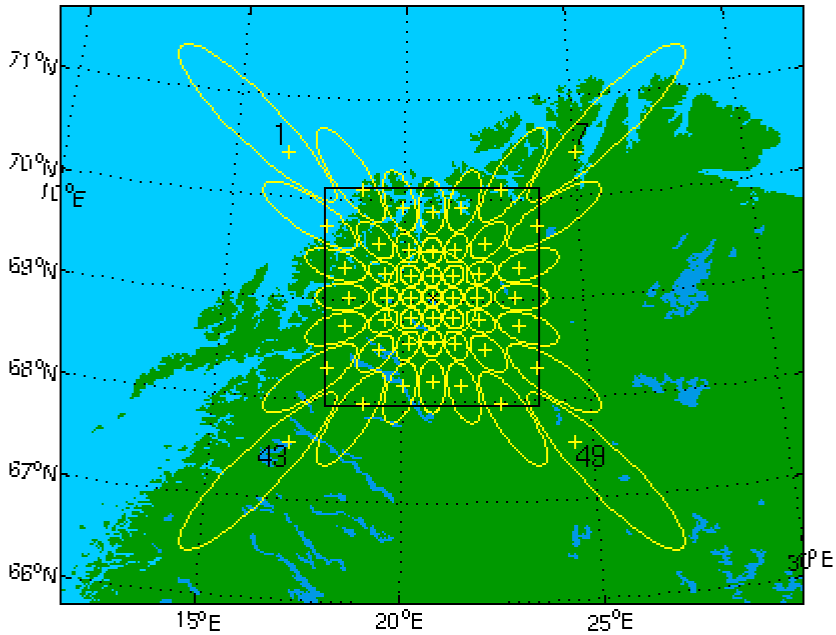

Fig. 3.3. IRIS Riometer Beam Projection-Kilpisjarvi-Finland.

(Courtesy Dr. Steve Marple, Lancaster University)

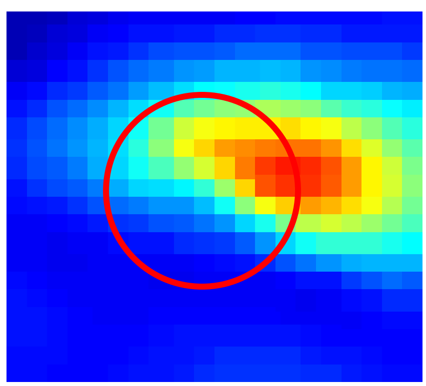

Fig. 3.4. An Absorption image measured by IRIS at 90 km altitude. The red circle indicates an opening angle of ±30° of a vertically looking wide beam riometer [Harrich et al. 2003]. One can see that an imaging riometer has a much better spatial (lateral) resolution.

For studies of the dynamics and structure of precipitating particles the AIRIS system (Andoya Imaging Riometer for Ionospheric Studies, http://alomar.rocketrange.no/iris-and.html) is in operation in Andenes, Norway (69.17°N; 16.01°E) since January 2006 at

38.2 MHz. An essentially similar system has been in use in Kilpisjarvi-Finland since 1990. Simultaneously measured riometer absorption data of vertical beam (25) at Andenes (AIRIS) and the oblique beam (8) at Kilpisjärvi (IRIS) (closest to Andenes) have a high overlap and their measurements are well correlated (Fig. 3.5).

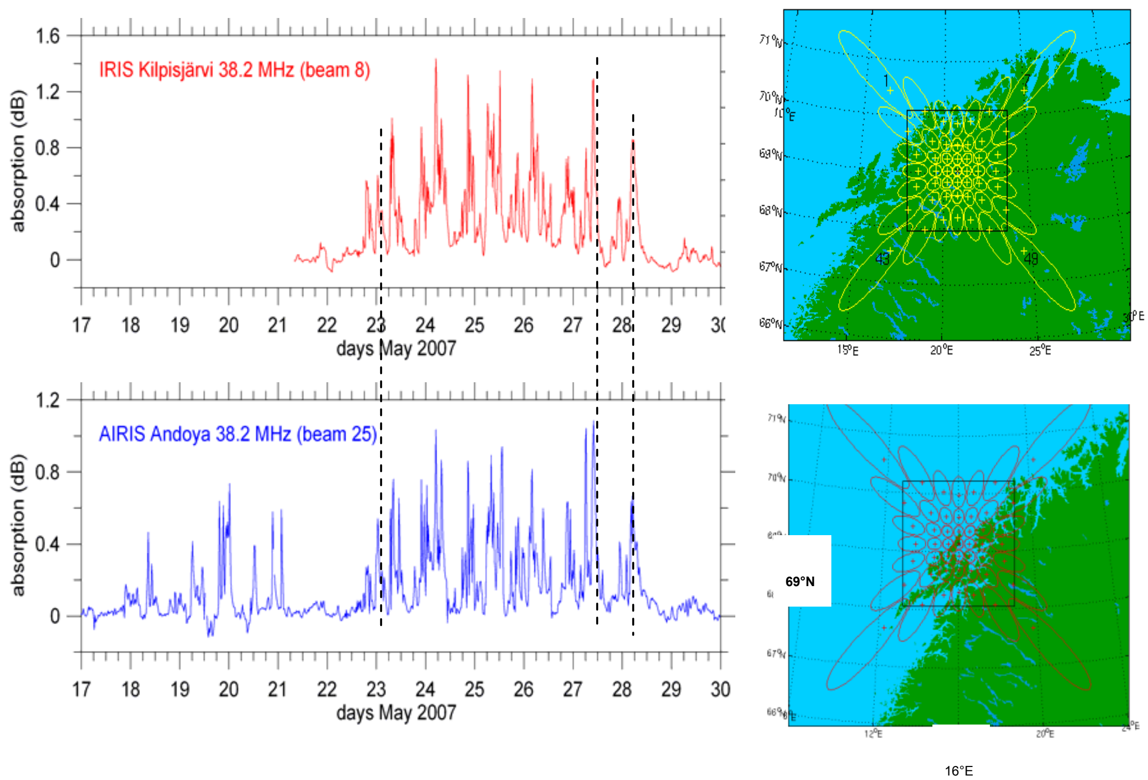

Fig 3.5. Simultaneously measured riometer absorption data of vertical beam (25) at Andenes (AIRIS) and the oblique beam (8) at Kilpisjärvi (IRIS) (closest to Andenes) are well correlated. (Courtesy Dr. Werner Singer, IAP)

3.4. Other observations (of the ionization) of the lower ionosphere

3.4.1. ALWIN MST Radar

On October 12th, 1998 a new VHF-radar was taken into operation at Andenes/Norway (69.17°N; 16.01°E) for investigations of the dynamics and structure of the troposphere, stratosphere, and mesosphere (Fig.3.6). Height profiles of the 3-D wind vector and of the radar reflectivity can continuously and unattendedly be derived by the Spaced-Antenna (SA) method and Doppler beam-Swinging (DBS) method [Latteck et al., 1999].

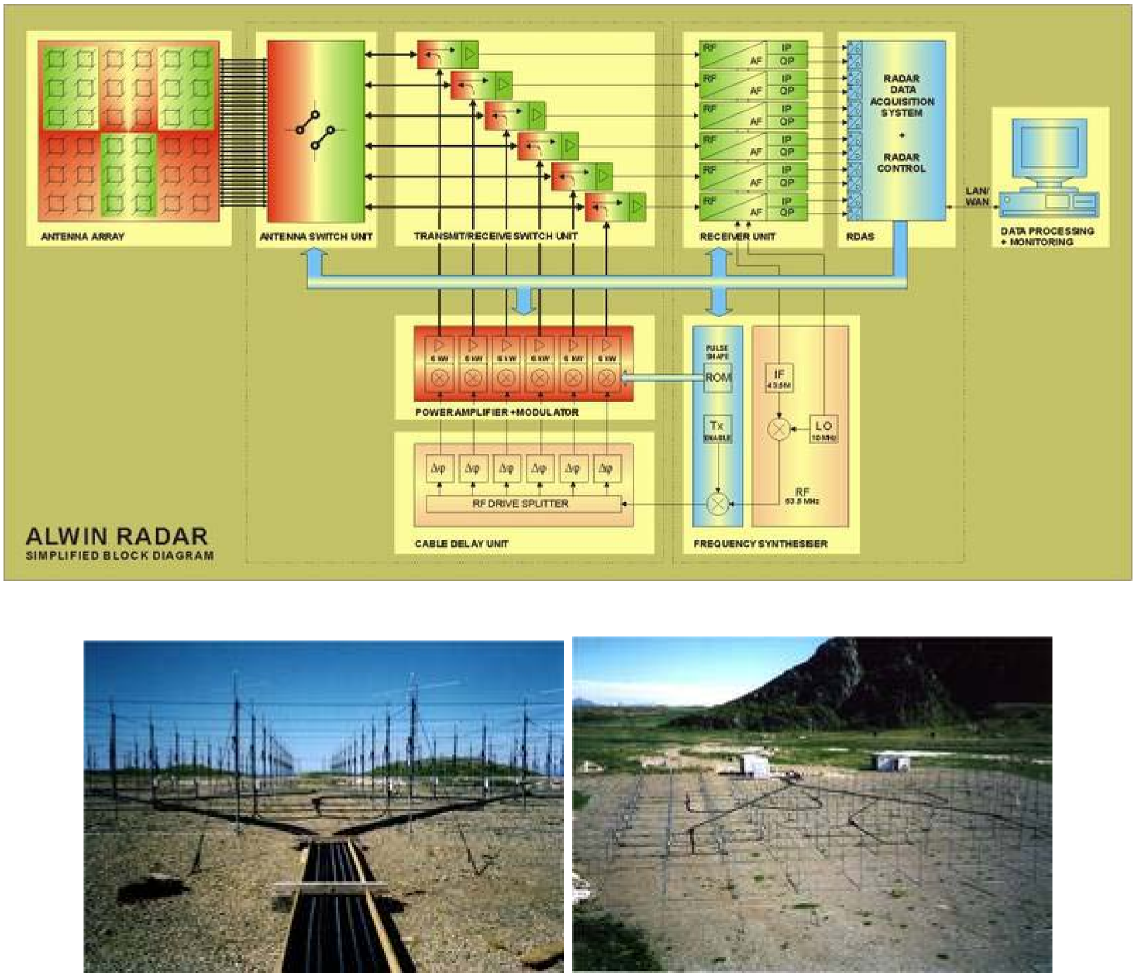

Fig. 3.6. Site and simplified block diagram of ALWIN Radar

The system is composed of four essential units. The completely transistorized transmitter consists of six units each with 6 kW transmitting power. The signals of each unit are transferred through a passive transmitting-receiving-switch to the antenna steering unit thus allowing an automatic operation of the transmitting/receiving antenna system in SA- and DBS-mode.

The transmitting/receiving antenna consists of 144 four-element-Yagi antennas grouped in quadratic subsystems of four antennas each and arranged in a 6x6 matrix. The distance between the individual antennas is $\lambda/\sqrt{2}$. The antennas are aligned by an angle of 45°concerning the North-South-axis thus ensuring that an identical antenna characteristic can be used in DBS-mode for zonal (East-West) and meridional (North-South) direction. In case of the SA-mode the antenna field for reception is subdivided in 6 individual fields consisting of 6 subsystems each. These 6 individual fields can be connected with maximum 6 receiving channels. In DBS-mode it is possible to swing the antenna beam in three zenith angles (7°, 14°, 21°) in the four directions North, South, East, and West. Such steering is made by a phase delayed feeding of the six antenna rows or columns in transmission case and in case of reception by a software supported post beam steering (PBS). Technical Parameters of ALWIN are as Table 3.

Frequency	53,5 MHz
Peak power	36 kW
Mean power	1,8 kW (at 5% Duty Cycle)
3dB beamwidth	6°
Pulse length	1 ... 50 μs
Pulse repetition frequency	< 50 kHz
Height ranges	(0,4) 1 ... 18 km (65 ... 95 km)
Height resolution	150 m, 300 m, 600 m, 1000 m
Time resolution	~ 1 min
Transmitted signal	impulse, complementary codes, Barker codes
Pulse shape	Rectangular, Gaussian, modified Gaussian

Table 3.1. ALWIN Specifications

The receiving system consists of 6 channels where the signals are pre-processed into their quadrature components. The following analysis of the raw data can be carried out online or as post process at the integrated host PC or at every other internet connected computer. A comprehensive software for the configuration and operational steering of the measuring experiments as well as for the diagnosis of the hardware permits a comfortable local and remote access to the system. By use of single and coded pulses in a combined mode, continuous wind profiles from 1 to 18 km can be estimated. In principle also measurements are possible within the boundary layer above 400 m by use of a modified SA-method.

In the mesosphere the ALWIN-VHF-Radar is mainly used for investigations of mesospheric radar echoes at polar latitudes in summer (PMSE) and in winter (PMWE). Since 2003 the ALWIN-VHF-Radar has the additional possibility to make investigations during selected measuring campaigns at ionisation traces caused by invading meteoroids using a separate transmitting antenna and spatial separated receiving antennas.

The system acquires data at a wide height range, at heights where atmospheric/ionospheric signals are present and at heights where the radio noise power is measured alone.

3.4.2. Saura MF Radar

Our knowledge of electron densities in 50 -90 km heights is relatively limited, partly because of observational limitations and partly because of difficulties in interpreting the observed ground-based data [Singer et al. 2005]. A new narrow beam MF radar has been installed in July 2002 close to the Andoya Rocket Range and the ALOMAR observatory to improve the ground based capabilities for studies of the dynamical status (small scale features, turbulence) of the upper mesosphere (Fig.3.7). The characteristics of radio wave scatterers can be studied in a wide frequency range by common volume observations with the ALWIN VHF Radar at 53.5 MHz (Latteck et al, 1999). The Saura MF radar is a joint experiment of the Andoya Rocket Range and the IAP. The main feature of the new radar is the antenna which is formed by 29 crossed half-wave dipoles arranged as a Mills-Cross. The spacing of the crossed dipoles is 0.7 wave lengths resulting in a minimum beam width of 6.4° [Singer et al. 2005].

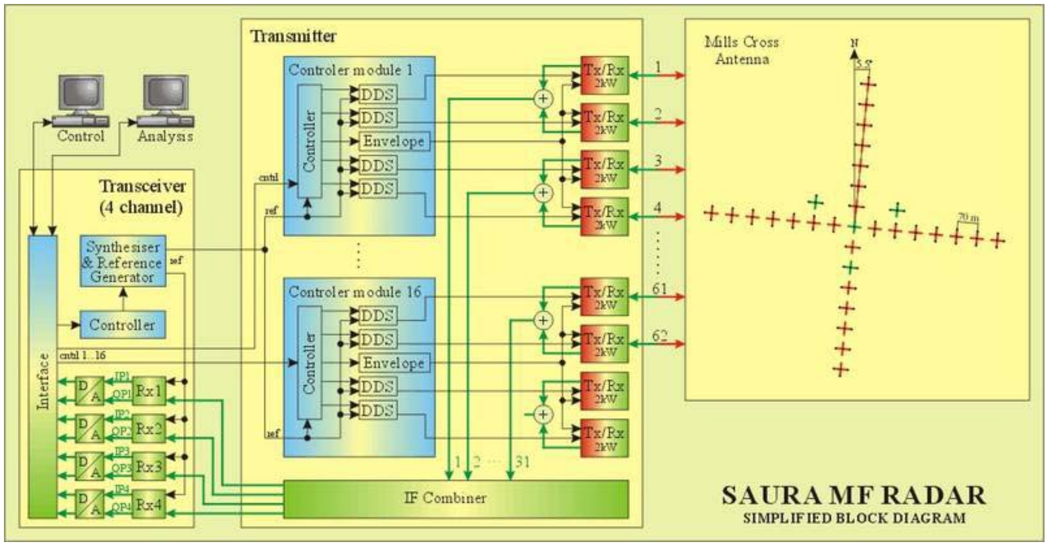

Fig. 3.7. Simplified block diagram of Saura MF Radar

Each dipole is fed by its own transceiver unit with a peak power of 2 kW (phase controlled on transmission and reception) providing high flexibility in beam forming and pointing as well as ordinary and extraordinary polarization mode operation for differential absorption and phase measurements. Off-zenith beams towards NW, NE, SE, SW at 7.3° or 17.2° can be formed. In addition, beams with different widths at the same pointing angle can be formed. For multiple receiver applications four independent receiving channels and two additional crossed dipole antennas are available. The system working at 3.17 MHz was put into operation in July 2002 applying spaced antenna observations and reached its full capabilities in April 2003. Technical Parameters of Saura are shown in Table 3.2**.** Beside wind observations it is possible to derive with the Saura-MF-Radar also turbulence parameters from the spectral width of the radar echoes as due to the small radar beam the disturbing influence of the horizontal wind can easily be eliminated. Also from the calibrated echo power, information about the atmospheric turbulence can be derived. Due to an alternating operation of the MF-Saura-Radar with different polarisations it is possible to derive electron densities between about 65 and 85 km by differential absorption and phase measurements. AIRIS riometer, ALWIN radar, and Saura Radar are shown in Fig. 3.8.

Frequency	3,17 MHz
Peak power	116 kW
Pulse width	7, 10, 13.3 μs
3dB Beamwidth	6.4°
Height range	50-94 km
Height resolution	1-1.5 km
Sampling resolution	1 km

Table 3.2. Saura Radar Specifications

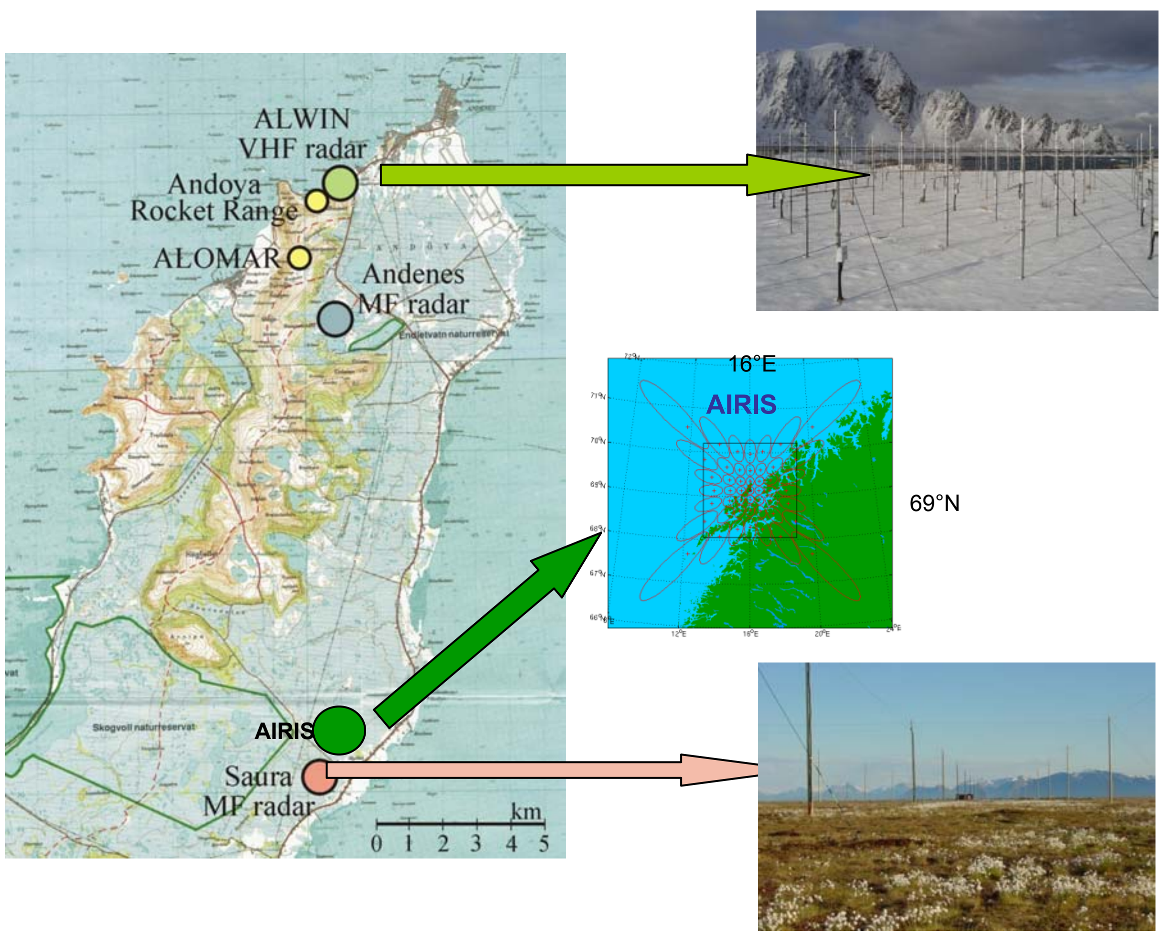

Fig. 3.8.AIRIS Riometer together with ALWIN and Saura Radars

(Courtesy Dr. Werner Singer, IAP)

4. ALWIN MST radar used as a narrow beam riometer

In previous chapters the principles of CNA measurement and riometry were illustrated. In this thesis, the CNA is estimated from the cosmic noise measurements carried out by a r*adar.*

4.1. Observations and Radar data

We use the vertical beam of the ALWIN narrow beam VHF Radar, as a narrow beam riometer (i.e. as a beam of an imaging riometer). Power values of radar signal from DBS files generated during several radar experiments (of 2003 to 2007) are the main source of data. Heights in the range 50 to 52.1 km are used (typically 7 heights in 300-m height steps). Since at this height range no atmospheric/ionospheric echo is expected, we expect that the radar receives only the Cosmic Noise background Power (CNP), and the transmitted radar signal echo will be used only as an indicator of enhanced ionization in the ionosphere.

4.2. Estimation of the Quiet Day Curve and of ionospheric absorption

QDC estimation needs a process of rejecting any spurious power value from the recordings. These spurious values can be generated by meteors, echoes from enhanced ionisation in lower heights, interfering radio waves, or other sources.

Meteors (and similar echo sources) have much stronger powers compared to the CNP; in practice they look like spikes in the records.

At any of the seven heights, the radar gives the power value (in dB) with a temporal resolution in the order of 1 to 3 minutes. To estimate the QDC, we need only one value at each moment (e.g. at any time bin, here of the order of half an hour). To reject the radar echoes like meteor echoes from the CN measurements, for any actual time, we select the upper quartile of the (seven) radar signals received from the (seven) heights for the CNP at the actual time, CNP(t) (i.e. we reject the two higher values, as if they are were very high, they may be meteor echoes, and if not, the third largest should not be much smaller than the rejected ones.). In this way we will have a time series of radar signal values (data points of signal Power) for the subject time duration.

Then we apply the following steps to estimate the QDC and the CNA.

I. Echo-power limiting, to remove power spikes (meteor echoes that may still exist)
II. Interference filtering (to reject the data when the radar signal is contaminated by other radio transmitters)
III. Geomagnetic activity Filtering (to reject the non-quiet conditions data, we use K-index, see section 2.2.2)
IV. Data Reduction (removing power values outside a logic range)
V. Estimating the QDC (by percentile method) and smoothing
VI. Calculating CNA(t)= CNP (no Abs.) –CNP(t) = QDC-CNP(t)

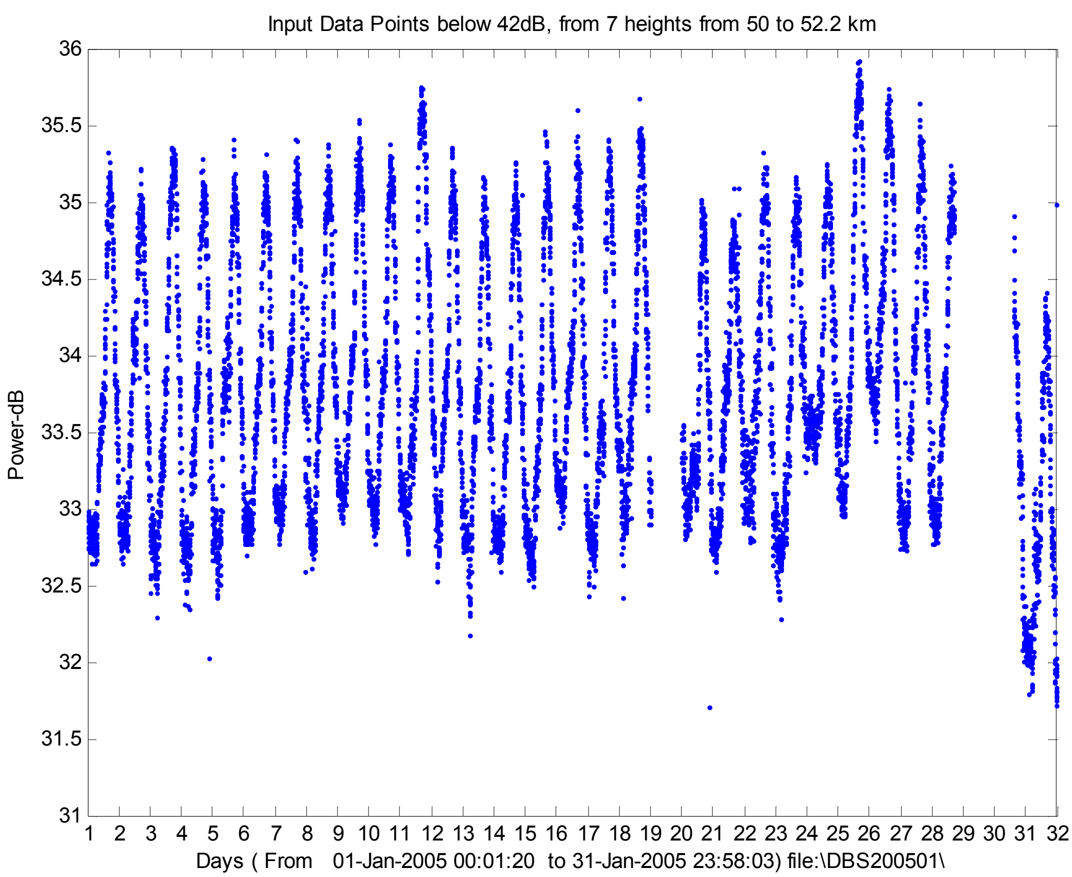

Fig. 4.1. ALWIN data points of Jan 2005.

4.2.1. Removal of spurious echo power spikes and interference

Despite the preliminary filtering by selecting the upper quartile of the seven heights, it is still probable that some meteor echoes are found in the data points. These echoes, which are normally quite few (by experience, less than ten echoes in one month data, i.e. less than 0.1% of the whole month data) and look like spikes in the data values can be partly rejected by setting an upper limit to the dynamic range of the data points. Fig. 4.1 shows the (upper quartile) data points (signal values) for one month of ALWIN observation at the height range 50-52.1 km during January 2005. Each point of this plot is the upper quartile of the seven signal values measured simultaneously at 50, 50.3, 50.6, 50.9, 51.2, 51.5, 51.8, 52.1 km heights; selected as to be the representative value of the CNP at that moment of time.

When the radar signal is contaminated by other radio transmitters the data can not be used for determination of the QDC.

In order to detect the interference-contaminated signal values from the data points, the ALWIN radar signal in the whole range of its work can be used. When there is a full-range effect, the radar is suspected to be affected by interference sources (Fig. 4.2).

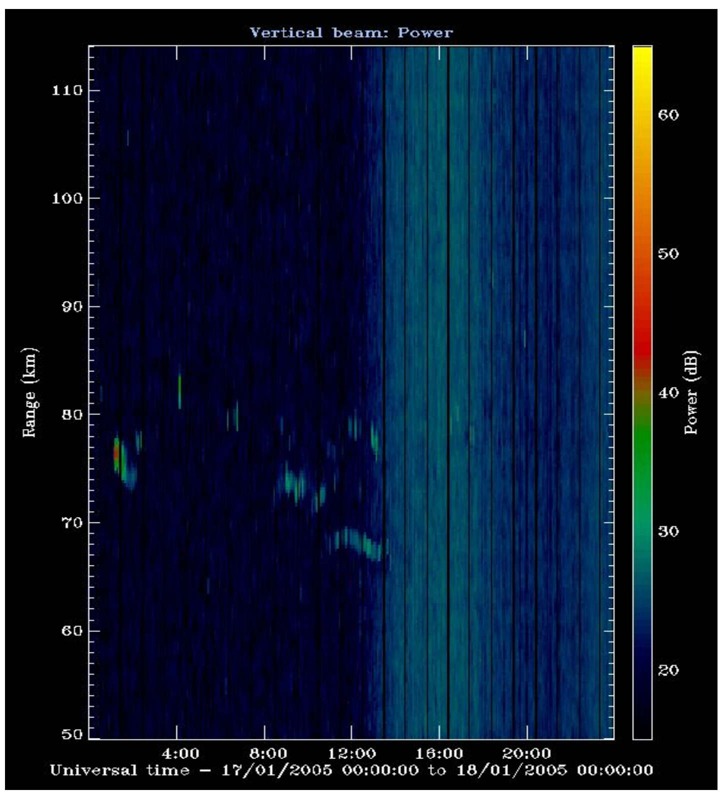

Fig. 4.2. ALWIN Vertical Beam Power (50 -114 km heights) during a day. (Whole-Range signature of) Interference is present from around 12:00 UT till end of the day.

We established an interference time map for ALWIN; When implemented, the program rejects the radar data of such interfered times in the QDC estimation process. The interference-filtered data points are set to a known low value to be easily rejected in the process of QDC estimation. (Data points shown in Fig. 4.1 will look like Fig. 4.3 after this filtering.)

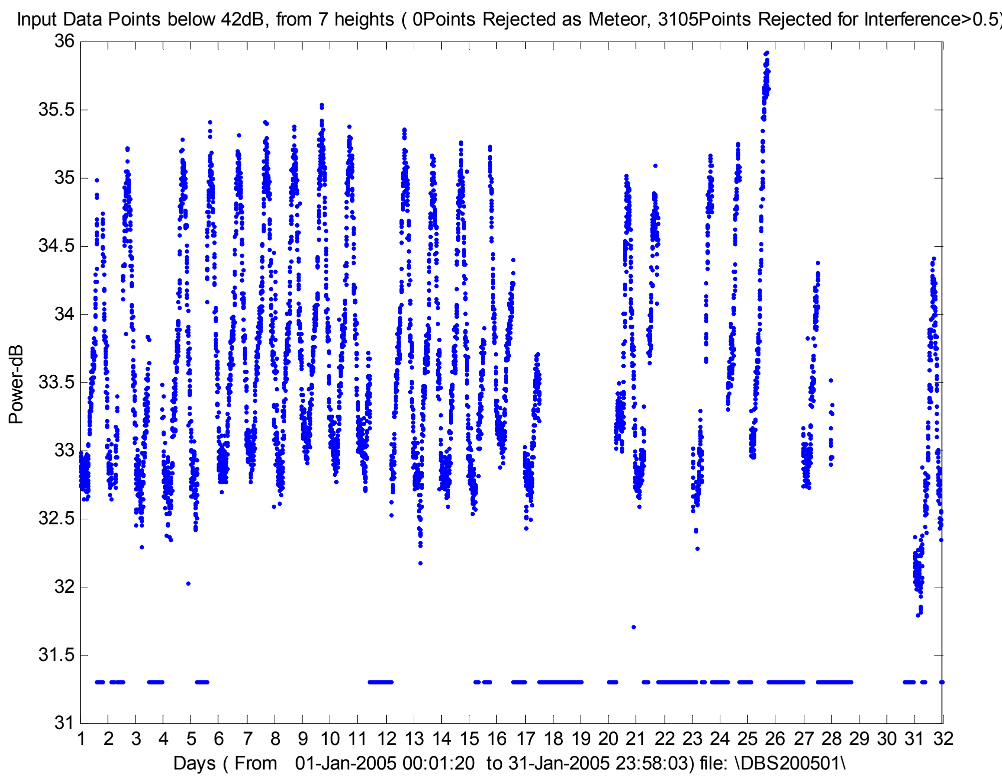

Fig. 4.3. Interference- filtered data points of Jan. 2005 (compare to Fig. 4.1)
The interfered data points are rejected down to 31.3 dB.

4.2.2. Filtering in respect to times of enhanced geomagnetic activity

To distinguish between quiet/ non quiet conditions, we use K-Index data measured at Tromso-Norway relatively close to the ALWIN Radar site. To reject the data coming from the non-quiet times, we remove the data corresponding to the times when the K-index is higher than 3 (see Fig. 4.4). After such a filtering, the data points of Fig. 4.3 will look like Fig. 4.5.

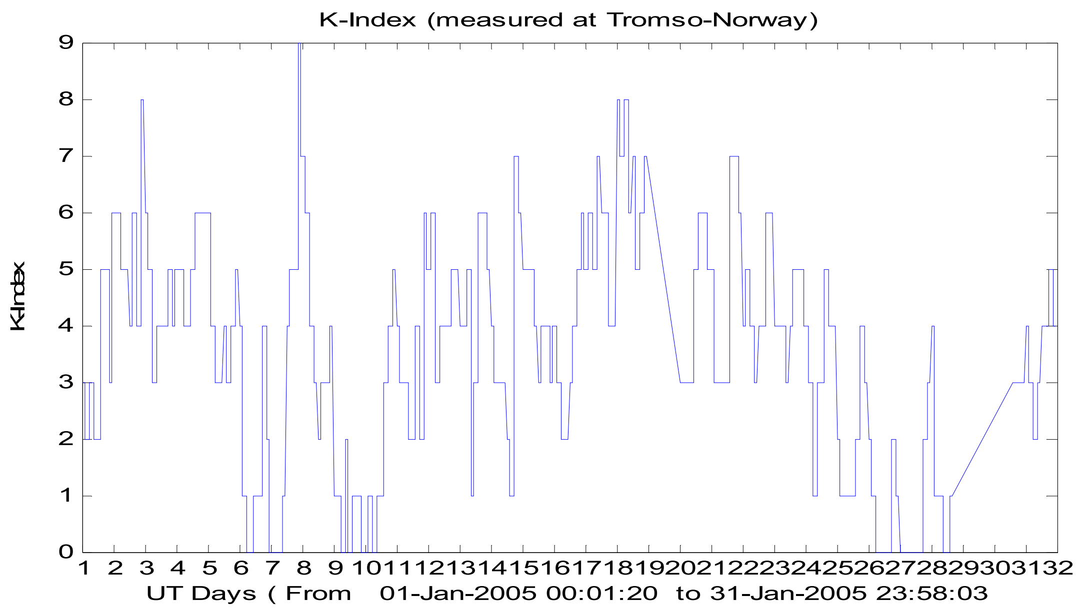

Fig. 4.4. The K-index time series generated at Tromso-Norway for Jan. 2005

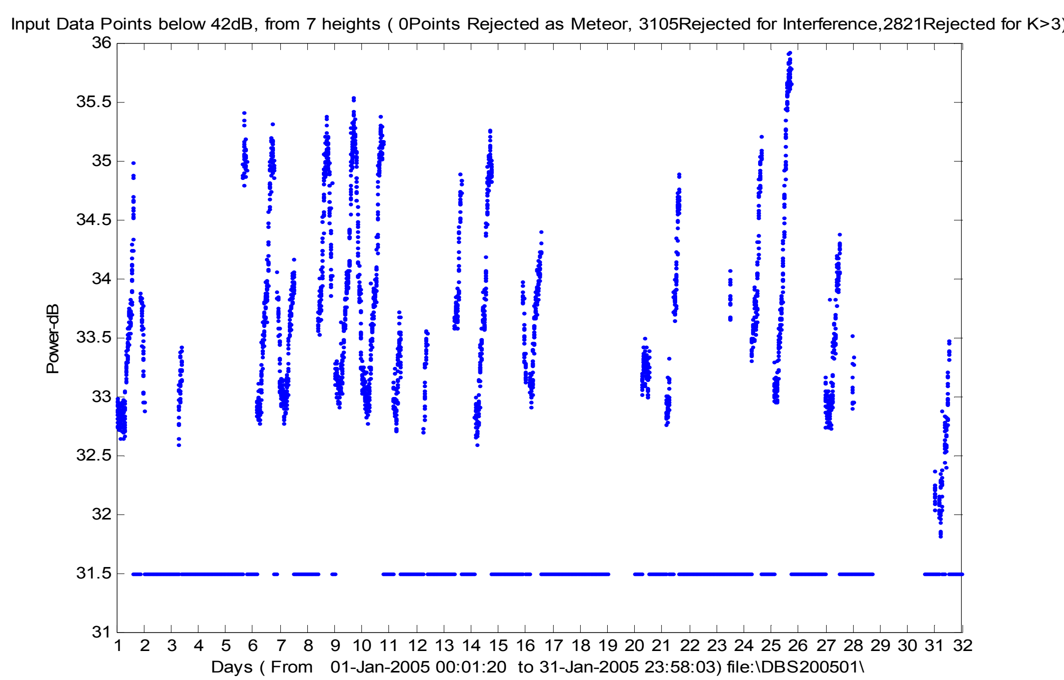

Fig. 4.5. K-index (and interference) filtered data points of Jan. 2005 (compare to Figs. 4.1, 4.3)

The interfered/Non-Quiet data points are rejected down to 31.5 dB.

The periodicity of the cosmic noise power is visible in Fig. 4.1, and one could see that the period of the curve of CNP is about one day; however, the exact period of this curve is one *sidereal day* (23h 56m 4s). To get a correct view of what the radar (or riometer) sees periodically when rotating with the earth and to determine the QDC, the day curves of several *sidereal days* of data ought to be overlaid on each other. Fig. 4.6 shows such an overlay of data points corresponding to the data shown in Fig. 4.3. Similarly Fig. 4.7 shows the K-index/ interference-filtered-data points (of Fig. 4.5) overlaid in local sidereal time (LST). The histograms of the three levels of data shown before, depicted in Figs. 4.8 and 4.9, show the impact of interference and solar/geomagnetic activity on the amount of data usable for the QDC estimation. The 20-minute Time-Bins used for the histogram will be used in the next steps of data reduction.

4.2.3. Data reduction and smoothing

The next step is to select a (say) 90% percentile upper envelope of the filtered data values. This is done by dividing the sidereal day into 20-minute time-bins and selecting the 90% percentile in each time bin. The 90% percentile curves of the raw data (Fig 4.1) and K-index/interference-filtered data (Fig. 4.5) are shown in Fig. 4.10 in red and green respectively. Even the latter shows some fluctuations that have roots in the quality of the data which has been used for the (Q)DC estimation. In this step we reduce the data values which do not fit in a logic region: In each time-bin, we calculate a lower and an upper limit and we reject all the data outside this two limits:

Lower Limit=Median of the bin-2* (Upper Quartile value of the bin - Median of the bin)

Upper Limit=Median of the bin+2* (Upper Quartile value of the bin - Median of the bin)

To do this, at first the median and upper quartile curves are calculated and then the two limiting curves are calculated and smoothed and finally the data are reduced by the above mentioned method. (The smoothing method used is a binomial weighted moving average with 1,4,6,4,1 weights).

After such a data reduction, the upper 90% curve of the Jan. 2005 data will look like the blue curve in Fig. 4.10.

The QDC estimated as above is then mildly smoothed by a binomial Weighted Moving Average (WMA) with 1,4,6,4,1 weights. (The QDC in Fig. 4.12 is the smoothed version of the blue curve in Fig. 4.10.)

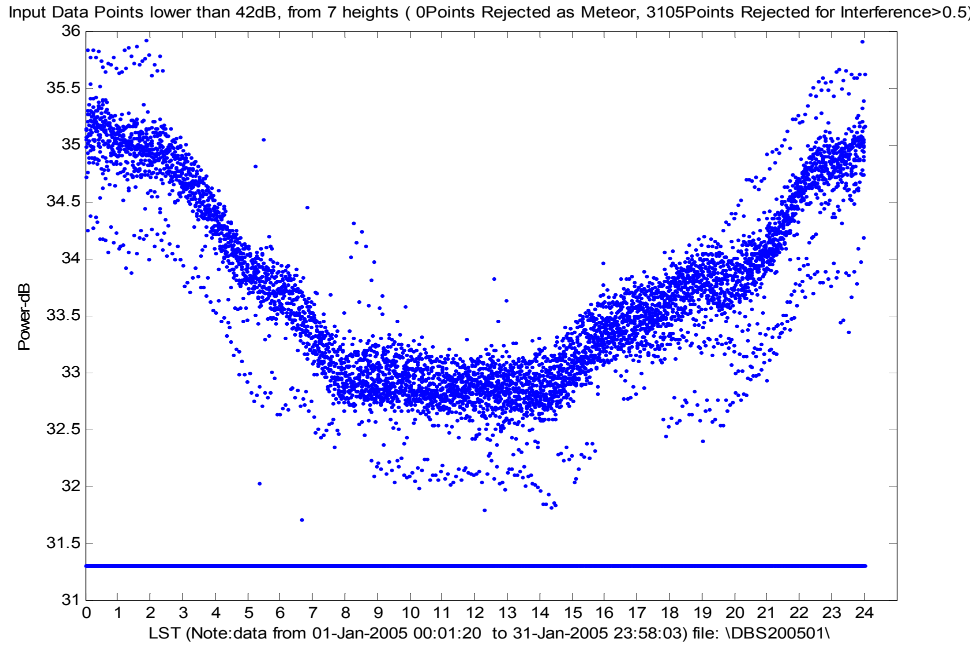

Fig. 4.6. The interference filtered data of Fig. 4.3 overlaid in sidereal time

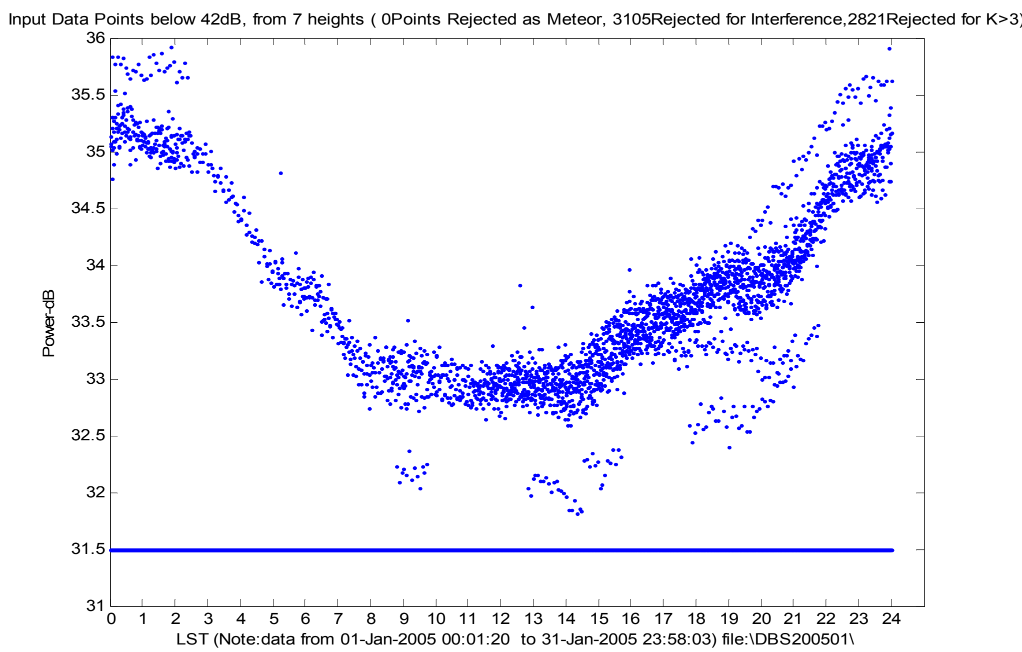

Fig. 4.7. The K-index/interference filtered data of Fig. 4.5 overlaid in sidereal time. The K-index/ interference filtered data points are rejected down to 31.5 dB.

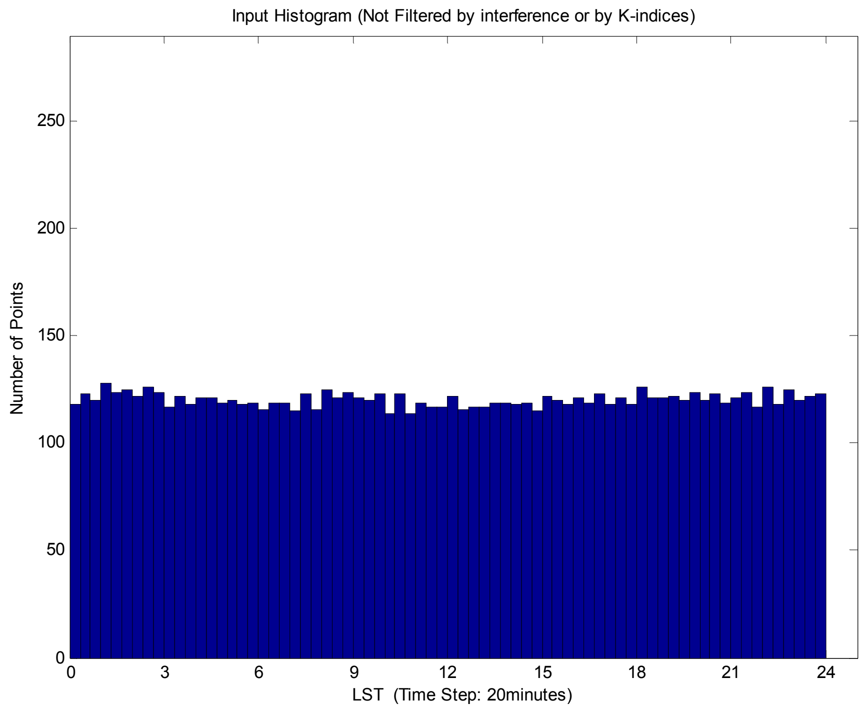

Fig. 4.8. Histogram of ALWIN data points- Jan 2005 (shown in Fig.4.1).

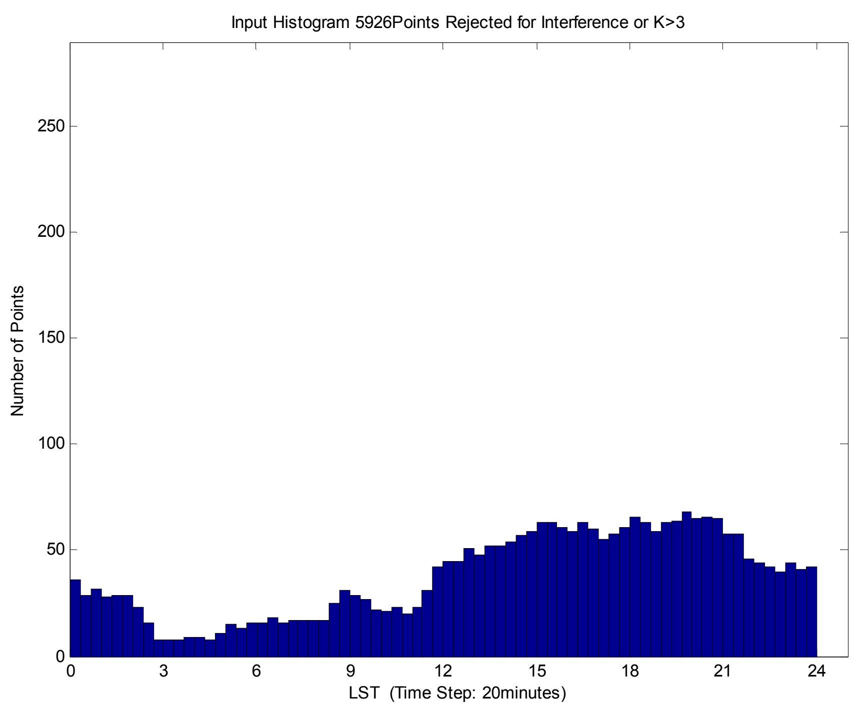

Fig. 4.9. Histogram of K-index/interference filtered data points- Jan. 2005 (see Fig. 4.5)

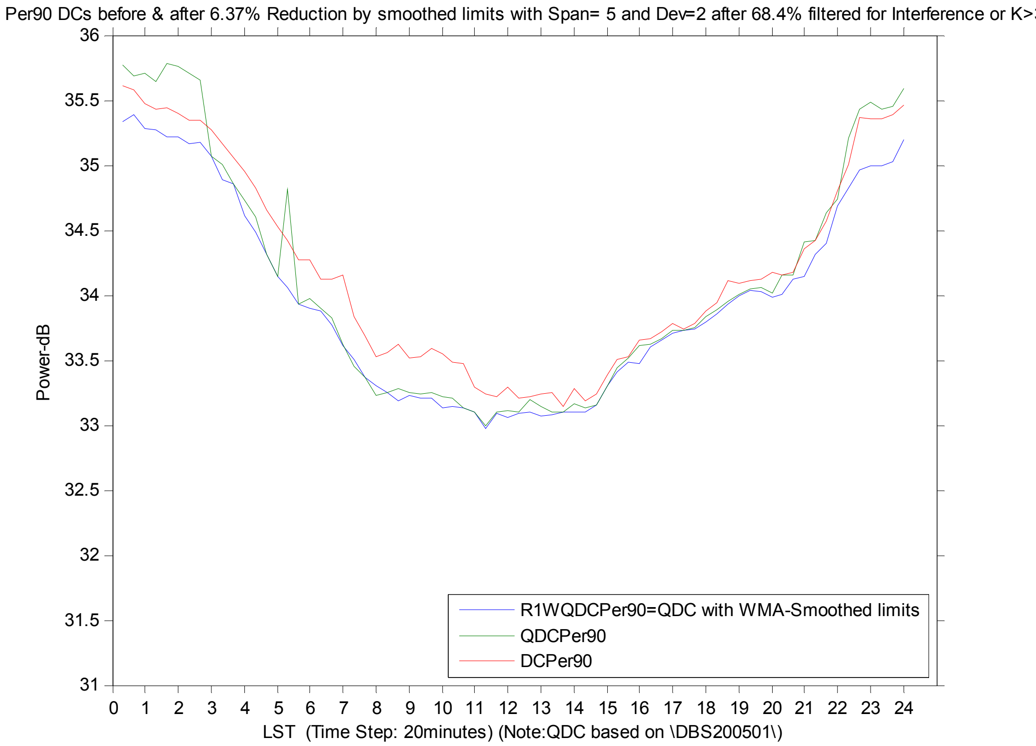

Fig. 4.10. The 90% percentile curves for the raw (red), K-index/interference- filtered (green) and reduced (blue) data points of Jan. 2005.

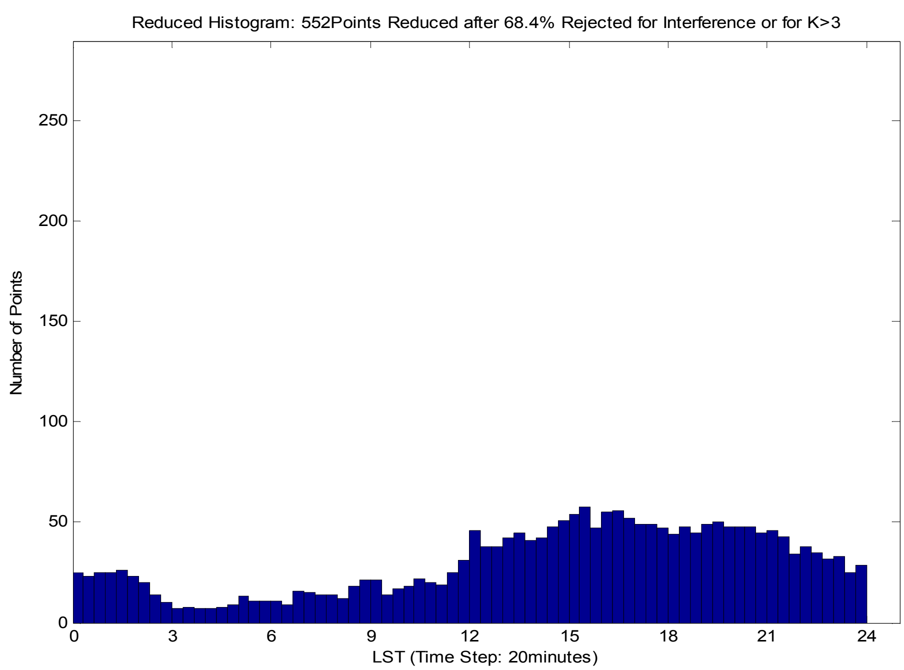

Fig. 4.11. Histogram of reduced K-Index-filtered Interference- filtered data points, Jan. 2005

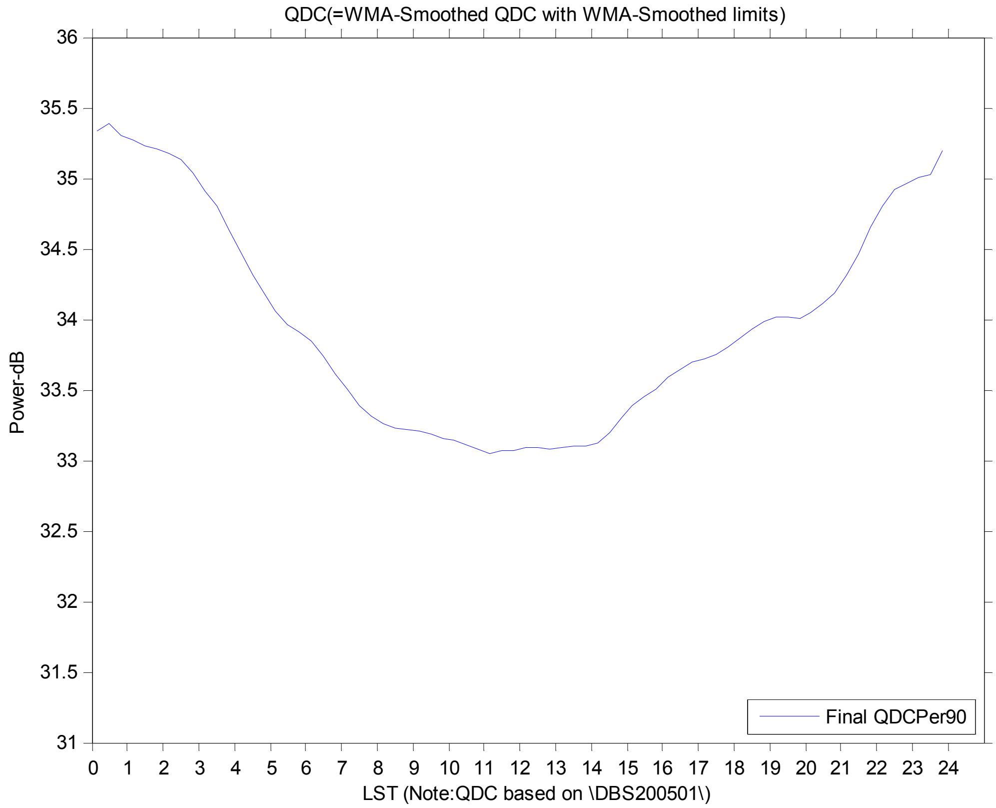

Fig. 4.12. The (final) QDC of Jan. 2005.

4.2.4. Calculating the Cosmic Noise Absorption

Any attenuation of the amount of received CNP relative to the QDC, is attributed to absorption introduced by the ionosphere. To calculate the CNA at any sidereal time (namely event time), the event day power curve is put on top of the QDC and the CNA is calculated from equation 3.4. To do this, the event has to be mapped to sidereal time first. Then CNA is calculated: $CNA(t) = CNP_{no\ Absorption} - CNP(t)$ or $CNA(t) = QDC - CNP(t)$, where CNP(t) is the event day curve (the power values recorded during the event day, arranged in sidereal time). Figs. 4.13 and 4.14 show the data of a day against UT and LST respectively and Fig. 4.15 presents the corresponding estimated CNA. This curve can be mapped back to UT for ease of use (Fig. 4.16).

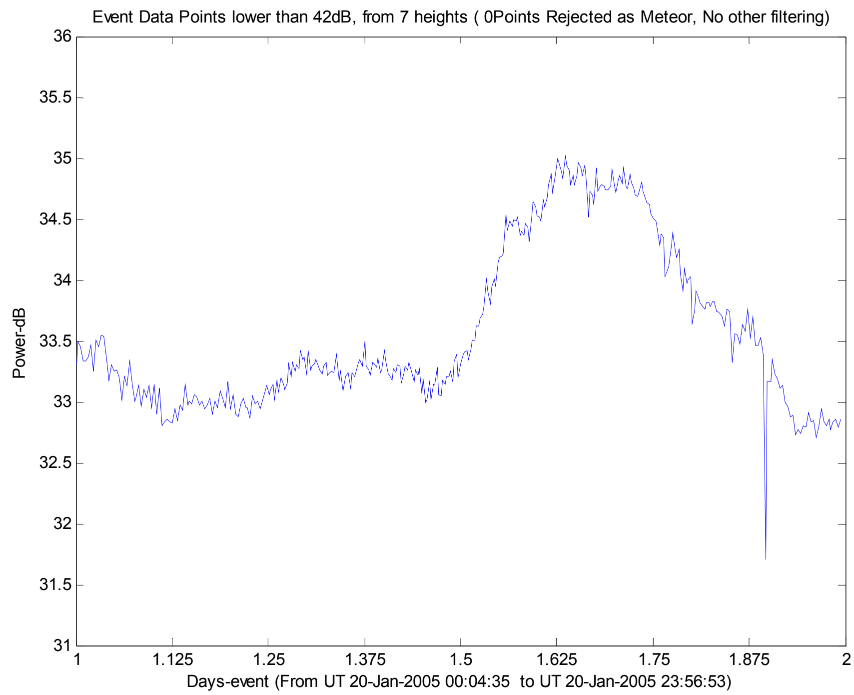

Fig. 4.13. ALWIN data of one solar day (UT)

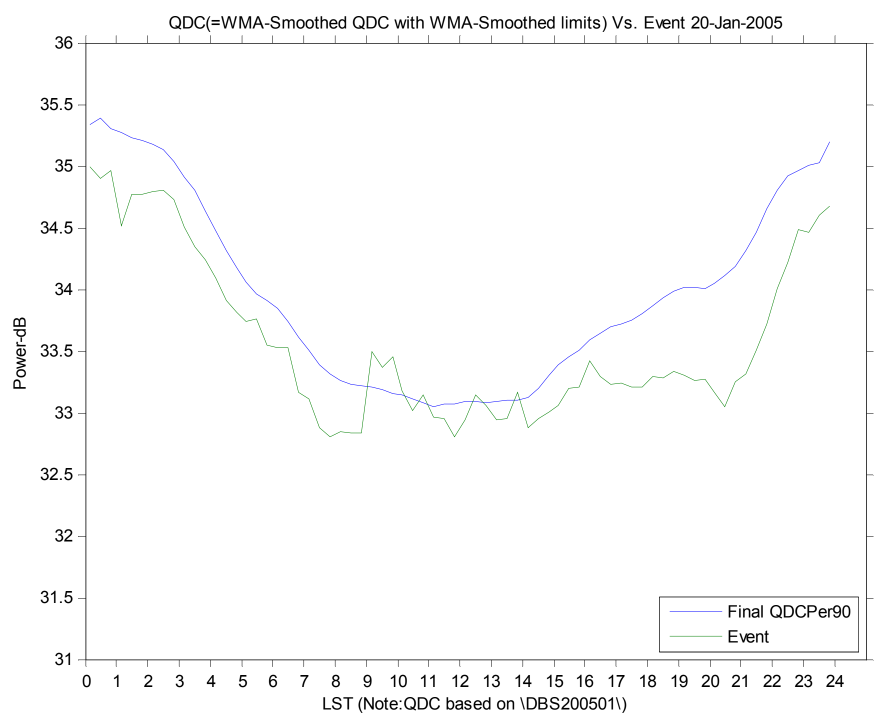

Fig. 4.14. ALWIN data of one Event day against LST (Green) and the QDC (Blue)

(The Event curve is smoothed also)

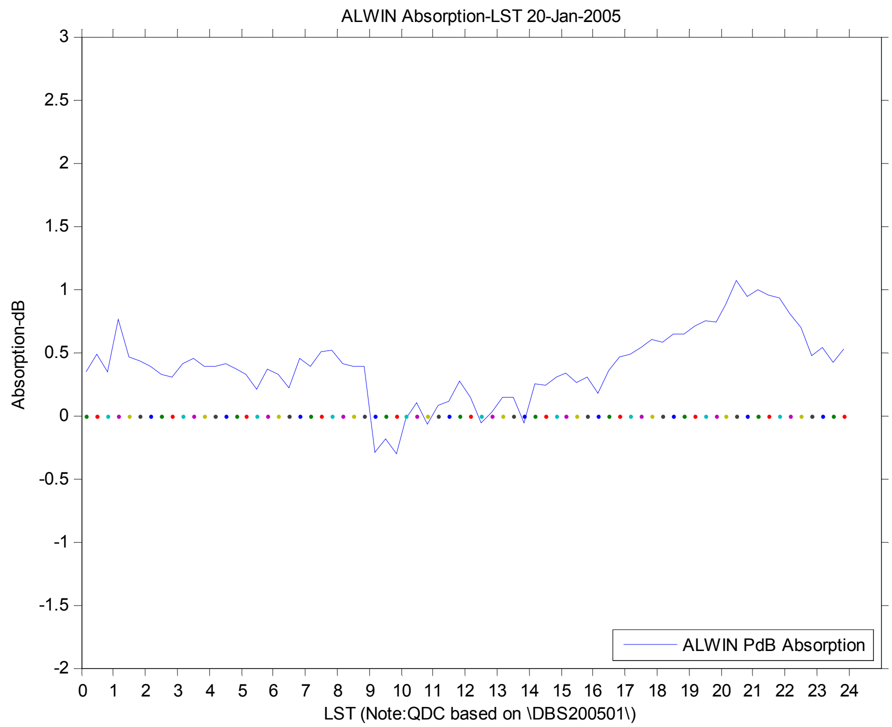

Fig. 4.15. CNA estimated for 20 Jan 2005 (against LST)

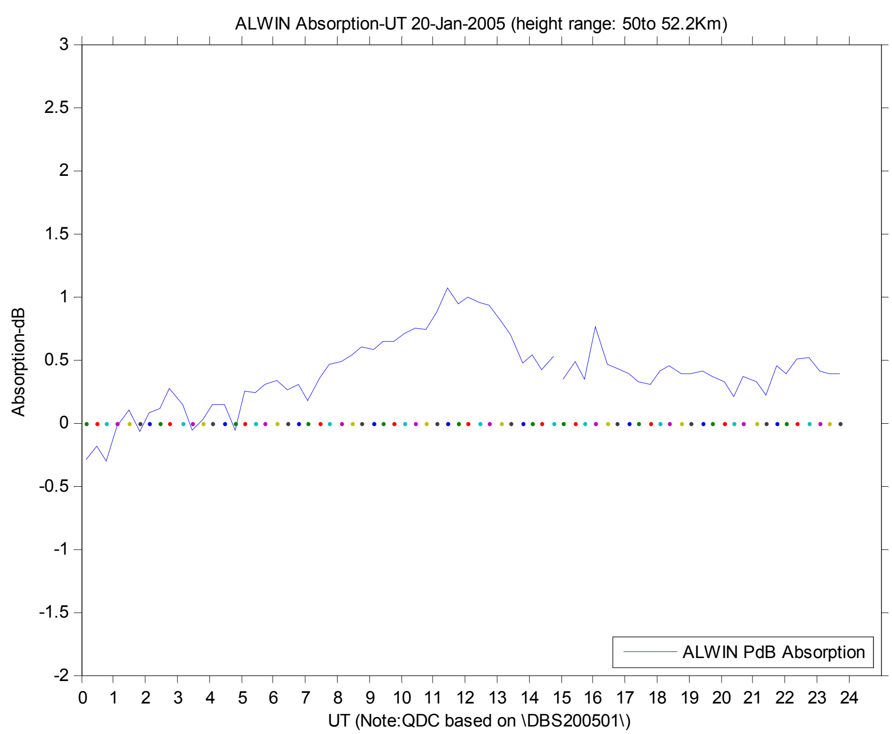

Fig. 4.16. CNA estimated for 20 Jan 2005 (against UT)

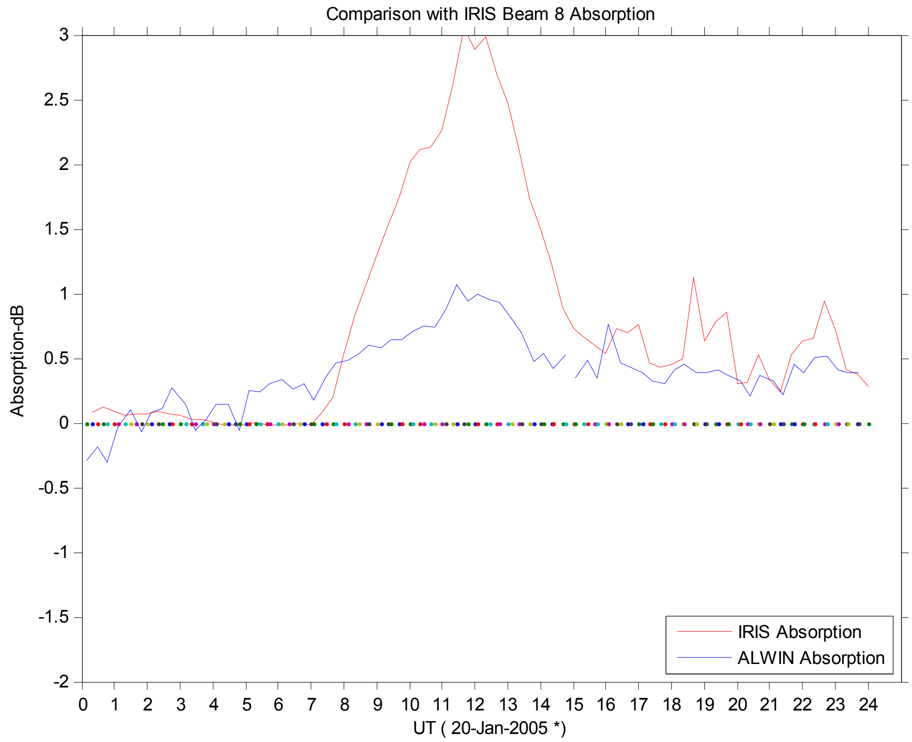

Fig.4.17. CNA estimated for 20 Jan 2005 by ALWIN at 53.5 MHz (Blue) and IRIS at 38.2 MHz (Red)

4.3. Comparison with common-volume observations of the riometer IRIS

Fig. 4.17 presents a comparison of the cosmic noise absorption obtained by vertical beam observations of the ALWIN radar and by oblique beam observations of the IRIS system (beam 8 collects data from the 90-km region above Andenes). Both data sets agree in their time evolution and the times of peak amplitude. The maximum absorption values observed on both frequencies (ALWIN - 53.5 MHz, IRIS - 38.2 MHz) also are in agreement as they fulfill the frequency dependence of cosmic noise absorption (for details see chapter 3.1). In the following frequency adjusted absorption are used.

4.3.1. Comparison with empirical and simulated riometer QDCs

The estimated ALWIN QDCs (e.g. Fig. 4.12) are in good agreement with the empirical QDCs and with theoretically simulated QDCs obtained by Friedrich et al. [2001] in terms of shape, peak-to-peak amplitude and variations of the curve (Fig. 4.18). (Their QDC simulation uses maps of the distribution of galactic noise and electron density measurements from rocket soundings at Andenes).

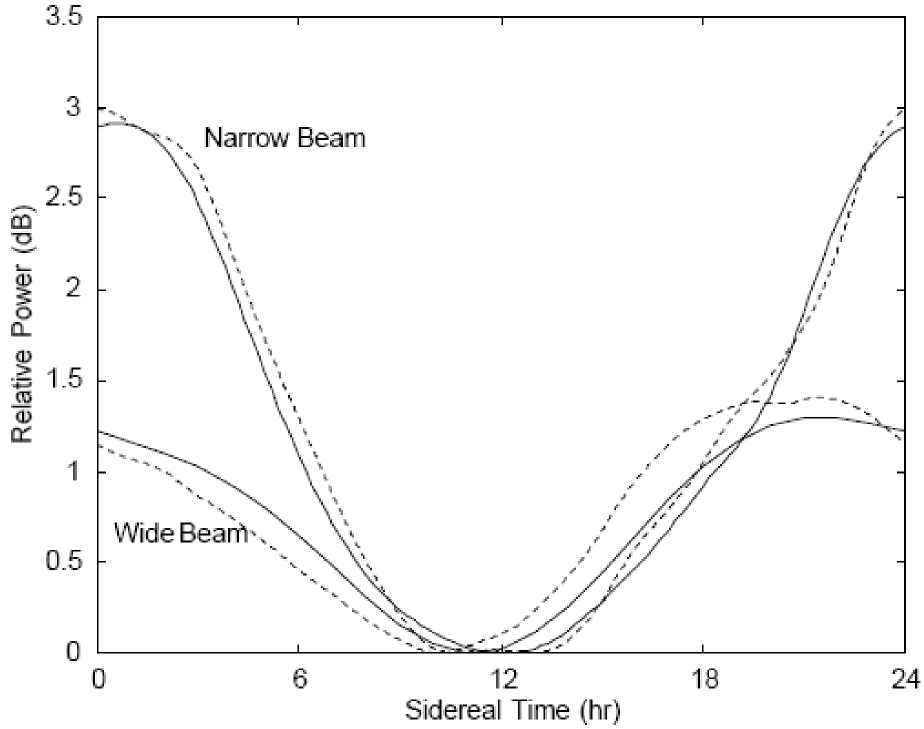

Fig. 4.18. Simulated (full lines) and observed (dashed lines) variation of received power (QDC) for a narrow beam riometer and a co-located wide beam instrument at Kilpisjarvi, Finland [Friedrich et al. 2001]. A winter period was chosen to assure absence of solar ionisation.

5. Results

As mentioned in previous chapters, the study of excess-absorption events was one of the first aims of riometry. In this chapter we show some examples of excess-absorption in the ionosphere and compare the estimated ALWIN CNA with other instruments.

According to magneto-ionic theories (Appleton-Hartree theory (Sen and Wyller, 1960) or extended Sen-and-Wyller theory (Friedrich et al.,1991)), radio wave absorption is to a good approximation proportional to the product of electron density and the frequency of collisions between electrons and neutrals. According to laboratory measurements (Phelps and Pack, 1959) the latter is proportional to pressure. The product of these two parameters thus maximises in the D-region. This maximum is generally between 70 and 100 km. Since pressure deviates only marginally relative to predictable “normal” values, the D-region electron densities must be responsible for variations of radio wave absorption [Friedrich et al. 2002].

Generally there are two sources of enhanced ionisation in the ionosphere: First, the ionization by protons coming directly from the sun during solar proton events and by X rays during solar flares, and second, the ionisation from the charged particles precipitating from radiation belts.

5.1. Solar proton event in January 2005

Fig. 5.1 presents the X ray and particle flux measurements of GOES satellite during a severe solar activity storm on January 16 to 23, 2005 with X_L-class X ray flares and proton fluxes with energies up to 100 MeV. Unfortunately ALWIN suffered from a severe interference during the most active times of the event (17, 18,19 Jan).

Fig. 5.1 also shows the electron number density measured on January 16 to 18, 2005 together with days of quiet solar activity. Electron density is increased at the maximum of the X ray flare (around 10:25 UT, 17 Jan.) by about one order of magnitude at altitudes below 65 km compared to undisturbed days. The still enhanced electron densities on January 18 in Fig. 5.1 are related to the slowly decreasing proton fluxes [Singer et al. 2005].

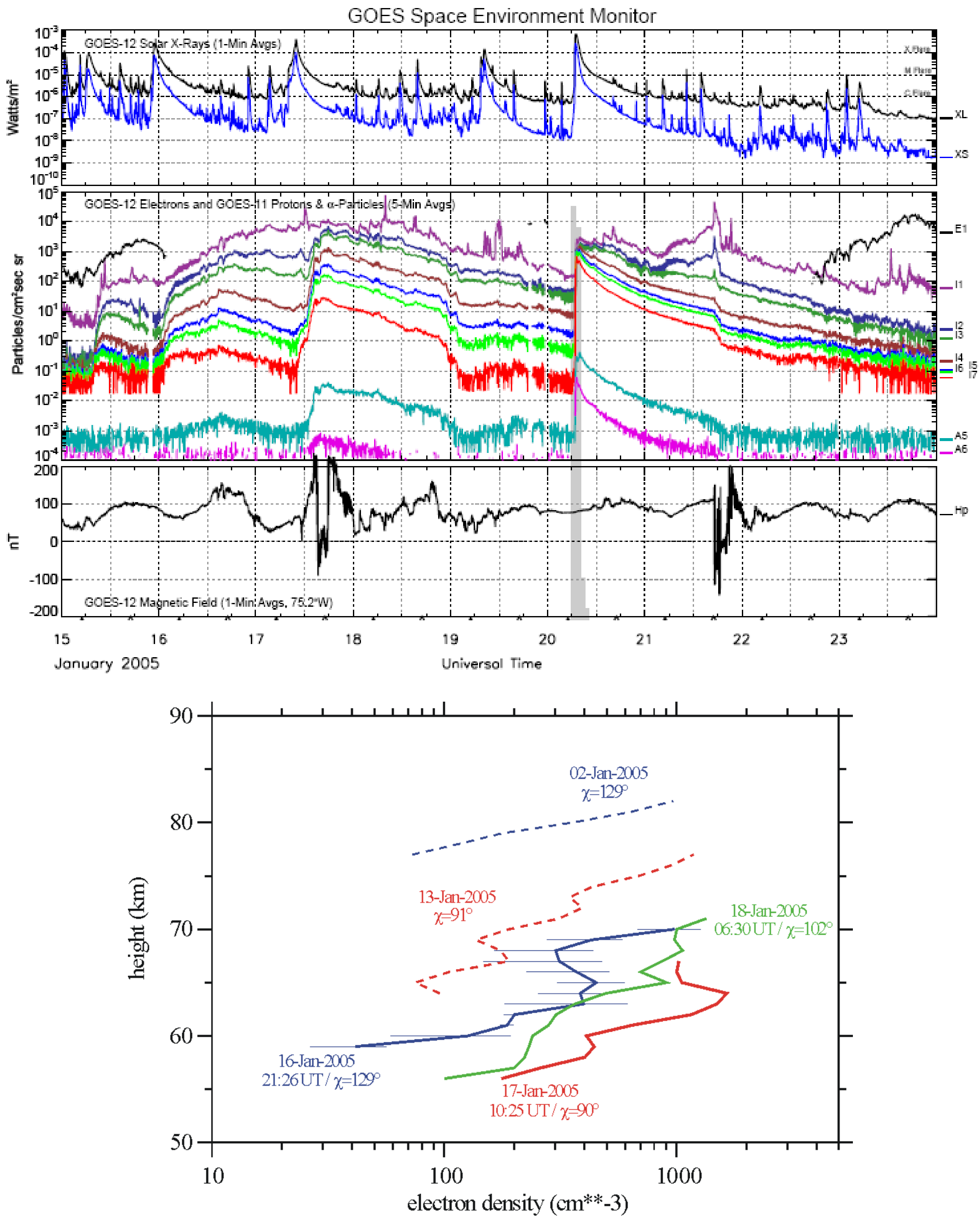

Fig. 5.1. X ray and particle flux measurements of GOES satellite, 15-23 Jan. 2005 (top panel) and D-region electron densities before, around, and after the maximum of the solar activity event on January 17, 2005 (lower panel). Electron densities on 18 January (06:30 UT) are still enhanced due to enhanced proton fluxes.

Fig. 5.2 depicts the derived cosmic noise absorption of the ALWIN radar and the absorption of the IRIS antenna beam pointing to Andenes. The IRIS absorption is adjusted to the ALWIN frequency. Simultaneous with the onset of the solar proton event the cosmic noise absorption of both experiments is increased by about 1 dB.

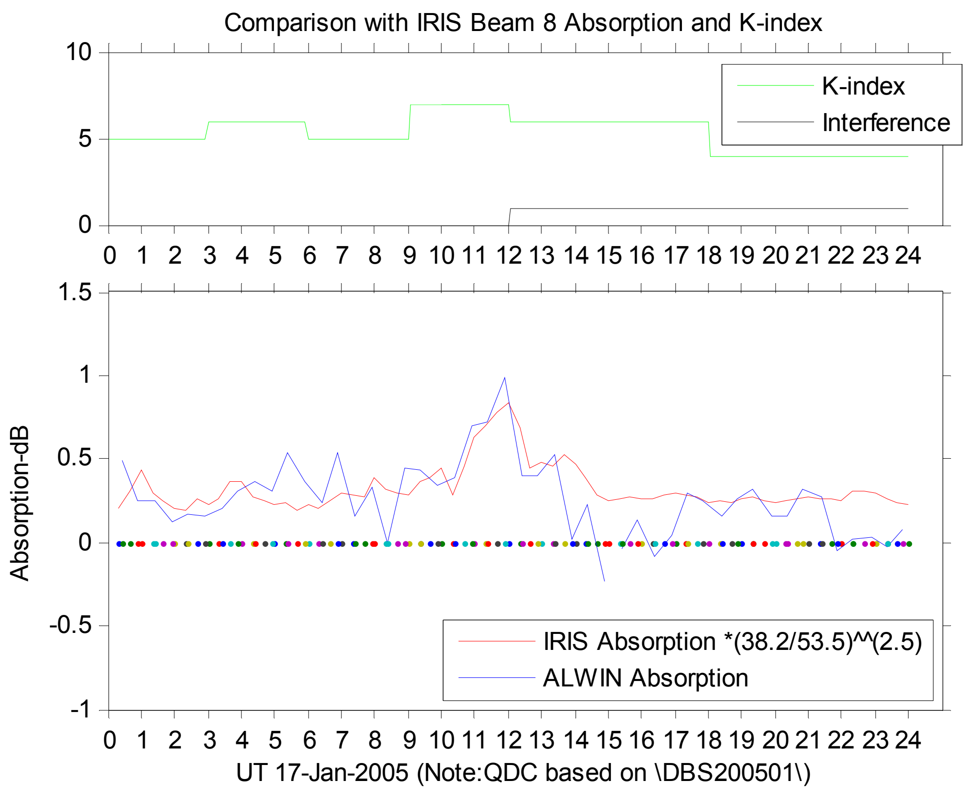

Fig. 5.2. ALWIN and IRIS cosmic noise absorption on 17 Jan.2005, the ALWIN measurements are influenced by interference from 12:00 UT onward (see also top panel).

Solar Proton Event on 20 January 2005

A solar flare on January 20, 2005 was connected with one of the largest solar protons events ever directly measured, taking only 15 minutes after observation to reach Earth (Fig. 5.1). The bottom panel of Fig. 5.3 shows ALWIN and IRIS CNA measurements along with precipitating high energetic particles fluxes of 40-80 MeV protons (top panel) and the K-index variations (middle panel) on 20 Jan 2005. The increase of the cosmic noise absorption observed by ALWIN and IRIS starts with the onset of the solar proton events and the CNA measurements reach their maxima around 11:30 UT.

The interfered/non-interfered event times of ALWIN are also depicted along with the K-index (zero level in the interference plot stands for negligible interference and level 1 indicates that there has been obvious interference on ALWIN).

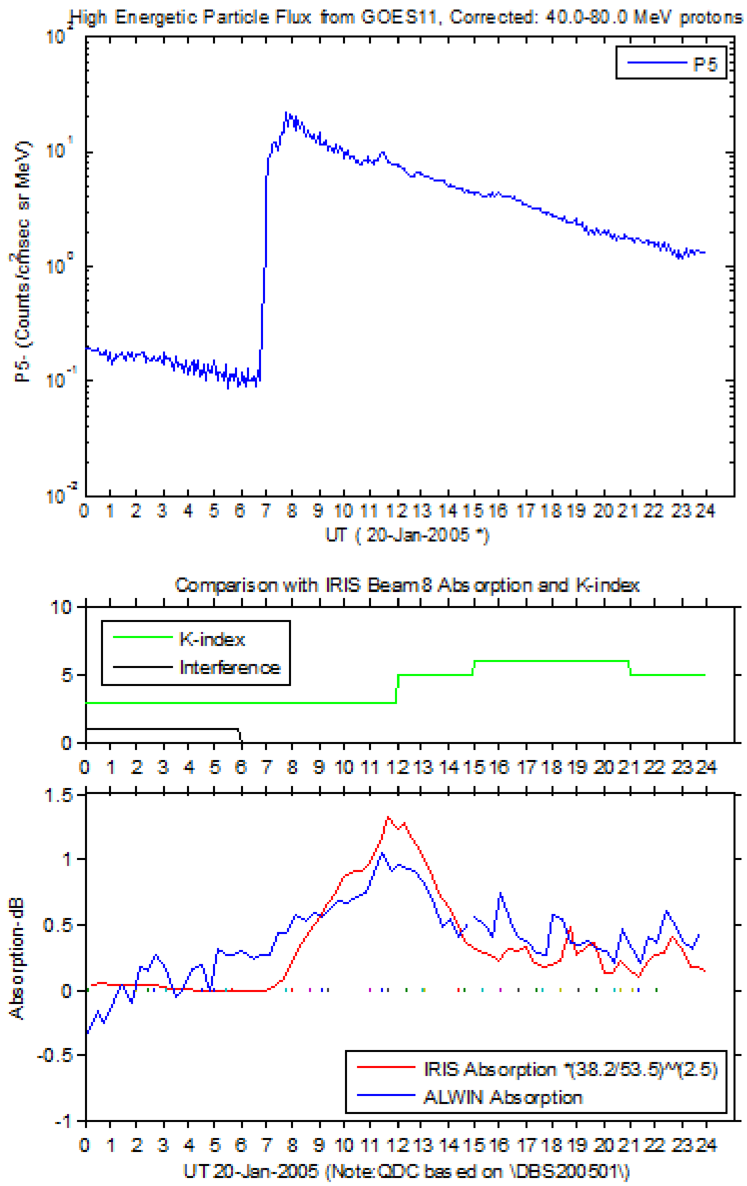

Fig. 5.3. ALWIN and IRIS CNA measurements (lower panel) along with particles flux data (40-80 MeV proton flux) from GOES Satellite (top panel) and the K-index variations (mid panel) on 20 Jan 2005. The steep enhancement in proton flux from the SPE coincides with enhancement in absorption.

Precipitating energetic particles on 21 January 2005

Fig. 5.4 shows the ALWIN estimated CNA along with IRIS and GOES measurements during 21 Jan. 2005. In this case the proton fluxes are smoothly decaying. The CNA increase during the second half of the day is caused by precipitating energetic particles as indicated by the enhanced geomagnetic activity (middle panel: K-indices larger than 5).

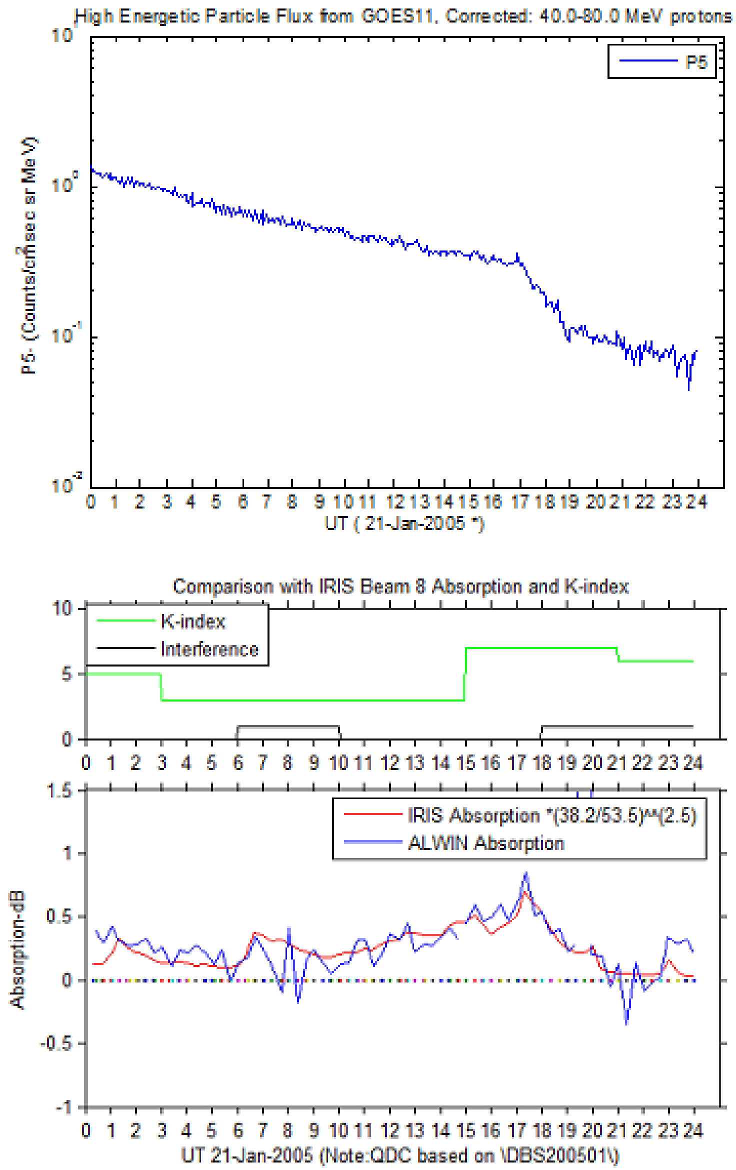

Fig. 5.4. ALWIN and IRIS CNA measurements (lower panel) along with particles flux data (40-80 MeV proton flux) from GOES Satellite (top panel) and the K-index variations (mid panel) on 21 Jan 2005.

This indicates that the CNA enhancement is resulted from precipitating energetic particles from the radiation belts and not directly from the sun. This process is stimulated by a geomagnetic storm peaking at around 17:00UT when the solar wind hits the magnetosphere, and this disturbance lets the particles pass the magnetic shield faster and accelerates the discharging of the belts into the lower ionosphere. (Note the magnetic field fluctuations and the faster decrease of the proton flux measured by GOES and the K-index enhancement before the peak of the CNA curves of ALWIN and IRIS.)

5.2. Solar Proton Event in Oct/Nov 2003

Solar cycle 23 was in decline during 2002–2003 as we moved from the season of flares to the season of persistent high speed solar wind streams. Though sunspot number maximum was in April 2000, the Sun continued to be very active [Space Environment Center 2002–2003]. In October/November 2003 one of the strongest Solar Proton Events (SPE) of the last four decades occurred. Fig. 5.5. shows 20 days of GOES measurements including this event (horizontal axis is Day number in 2003) and Fig. 5.6 presents more details on the part of the event in November.

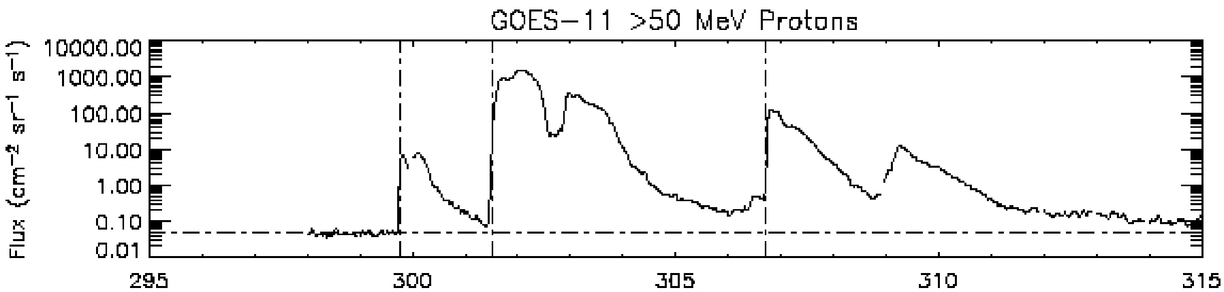

Fig. 5.5. GOES 11 data of >50 MeV proton fluxes during a series of solar proton events during 22 October to 10 November 2003 (After *Clilverd et al.* [2006]).

A proton flare (type X) occurred on the sun on 28 October 2003 (day 301) at 11:10 UT. In terms of X ray emissions it was one of the most intense flares of the cycle 23. A coronal mass ejection was observed at 10:54 UT, and within the magnetosphere, the flux of energetic protons began to increase at 11:50 UT. This flux peaked at 00:15 UT 29 October, lasted during 30 October, and the event ended about 13:10 UT on 1 November.

Fig. 5.7 shows calculated atmospheric ionization rates determined from the GOES-11 proton fluxes for the period 26 Oct-7 Nov 2003 using the Sodankylä Ion Chemistry (SIC) model [*Clilverd et al.*, 2005a]. Particle precipitation results in enhancement of odd nitrogen (NO_x) and odd hydrogen (HO_x). NO_x and HO_x play a key role in the ozone balance of the middle atmosphere because they destroy odd oxygen through catalytic reactions. SPE-produced ionization changes tend to peak at about 70 km altitude.

Figs. 5.8 to 5.11 present the CNA estimations of ALWIN and IRIS during some days of the event.

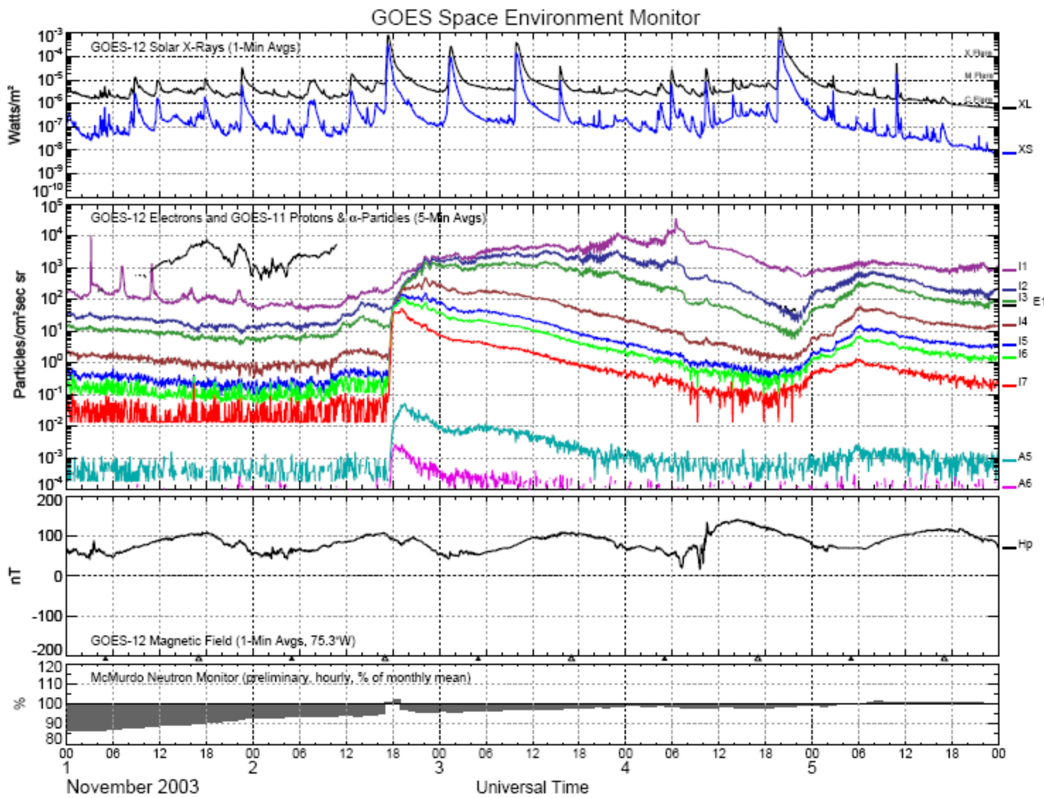

Fig. 5.6. X ray and solar proton fluxes from GOES measurements for the period 1 -5 November, 2003.

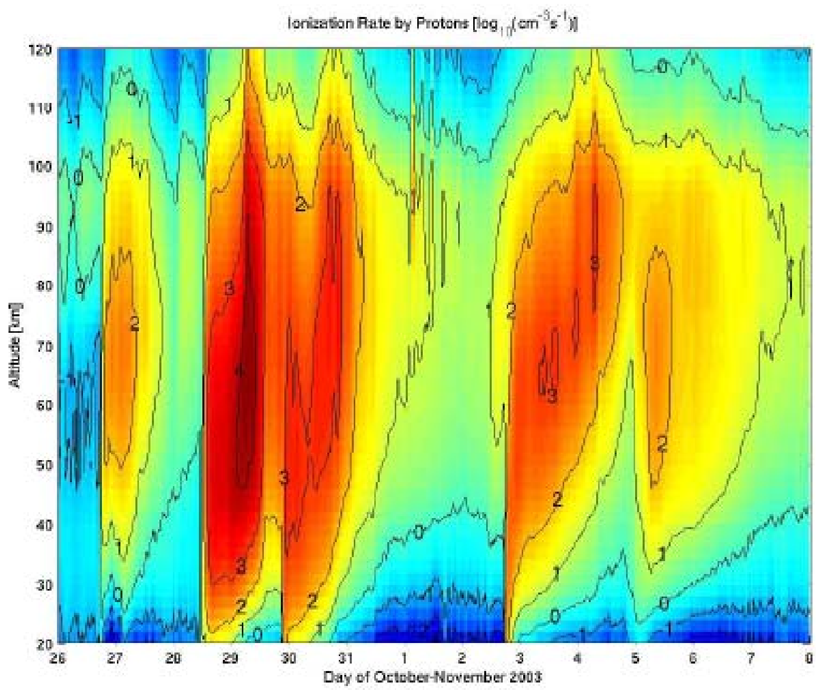

Fig. 5.7. Ionization rates in the atmosphere calculated using SIC based on GOES-11 proton flux measurements for the period 26 October to 7 November 2003 (after Verronen et al., 2005).

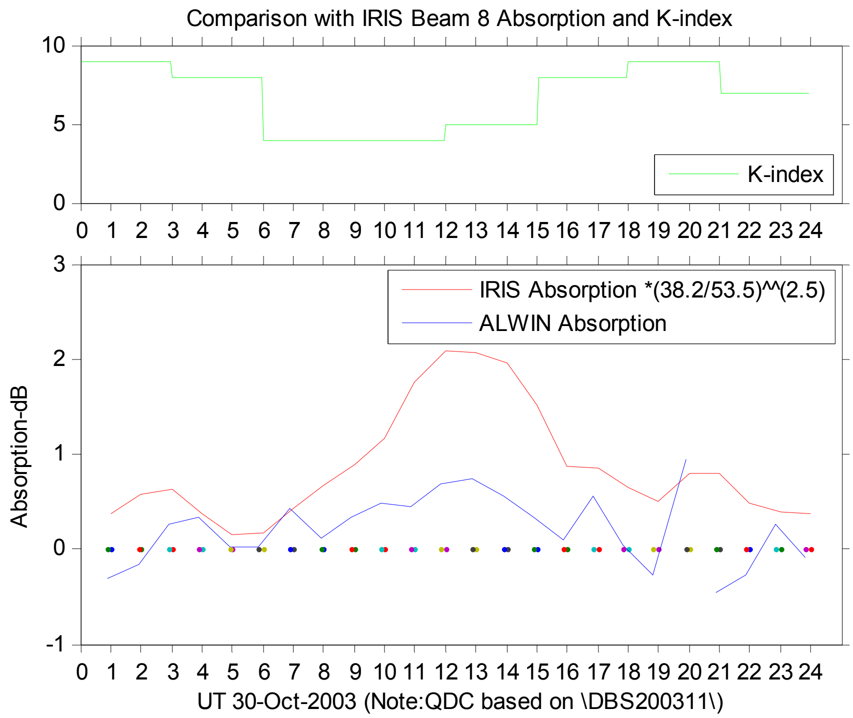

Fig. 5.8. Enhanced CNA in ALWIN and IRIS due to Precipitation of Energetic Particles

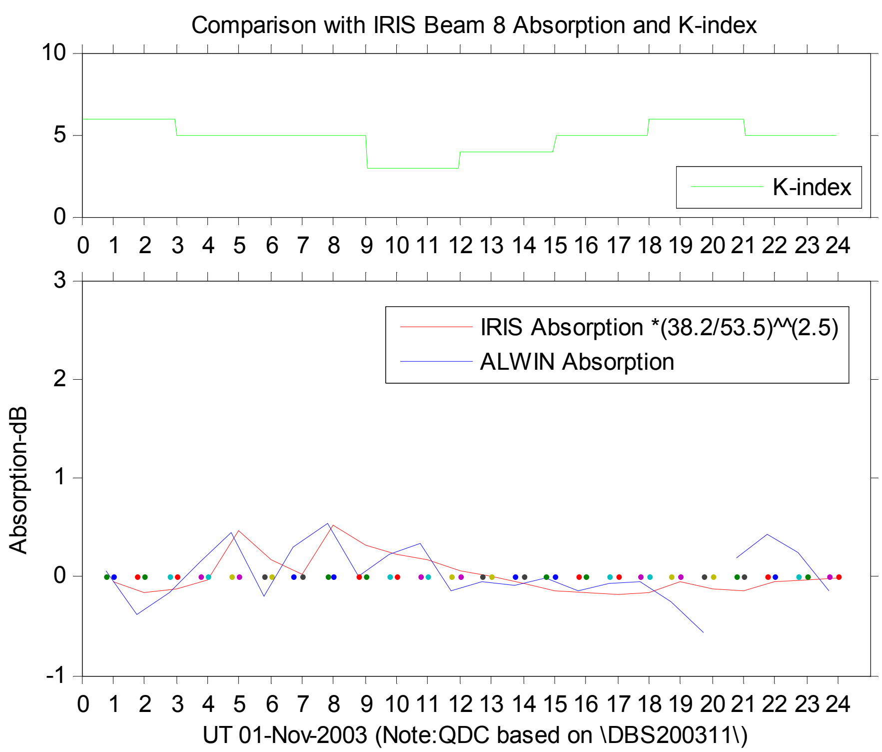

Fig. 5.9. ALWIN and IRIS CNA measurements on 1 Nov. 2003

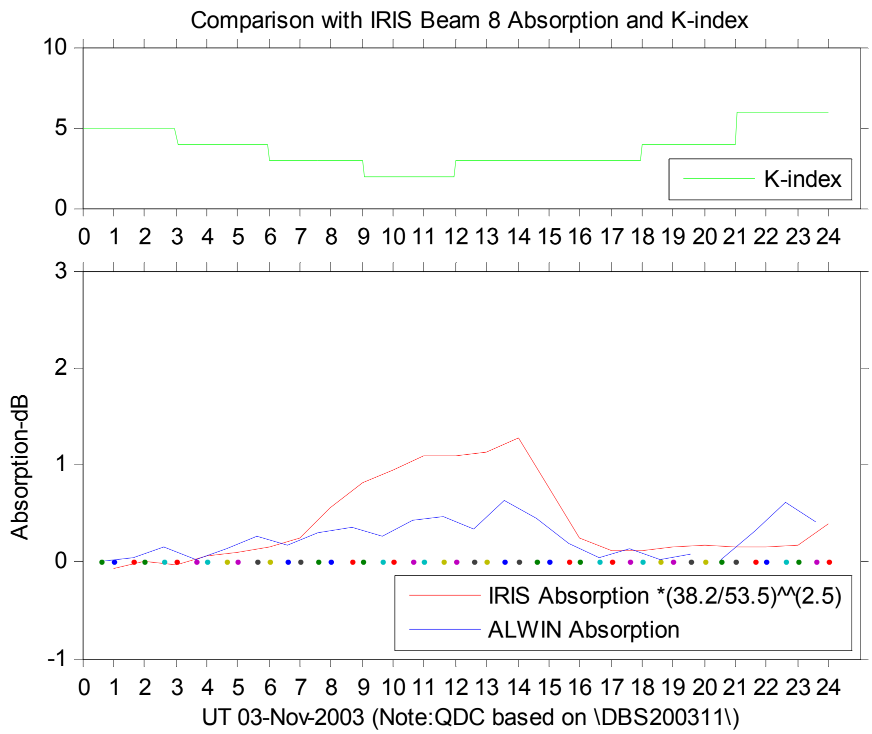

Fig. 5.10. Two X-Flares around 2:00 UT and 10:00 UT lead to enhancement in the ionization and the CNA.

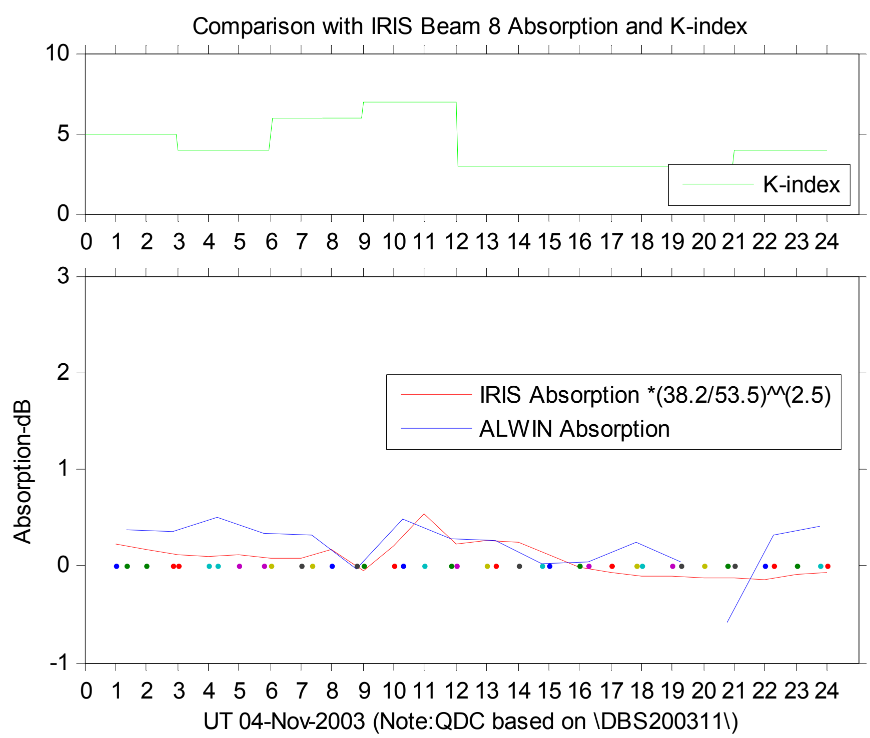

Fig. 5.11. At around 9:30 UT, X rays from an M-flare enhance the ionization and a following geomagnetic disturbance stimulates the proton discharge from the belts into the ionosphere, both leading to CNA enhancement.

5.3. Solar Proton Event in May 2007

The occurrence of other mesospheric phenomena which rely on enhanced ionization at altitudes below about 95 km can also be studied in relation with geomagnetic activity and related cosmic nose absorption. Strong radar echoes are observed by VHF radars preferred in winter at altitudes below of about 80 km so called polar mesosphere winter echoes (PMWE). The appearance of these echoes is well correlated with magnetically disturbed conditions and enhanced riometer absorption (Fig. 5.12) as sufficient is required to produce radar backscatter at these altitudes. Fig. 5.13 presents as example the cosmic noise absorption derived from the measurements of the ALWIN radar (vertical beam) and the riometers AIRIS (vertical beam) and IRIS (beam 8 - above Andenes). The absorption maxima detected by the diferent experiments agree well in appearance time and magnitude. The assumed exponent of 2.5 of the power law approximates well the frequency dependence of the cosmic noise absorption.

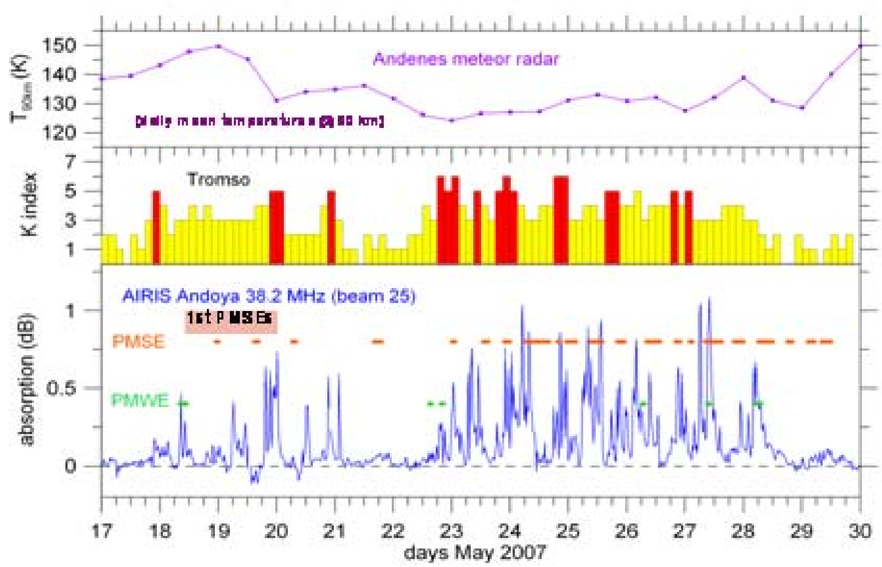

Figure 5. 12. Bottom panel: Occurrence of polar mesosphere winter echoes (PMWE) and polar mesosphere summer echoes (PMSE) after observations of the ALWIN radar and cosmic noise absorption of AIRIS. Middle panel: geomagnetic activity depicted by the K-index from Tromso. Top panel: Temperature at 90 km, PMSE generally appear at temperatures below 150 K (courtesy Dr. W. Singer).

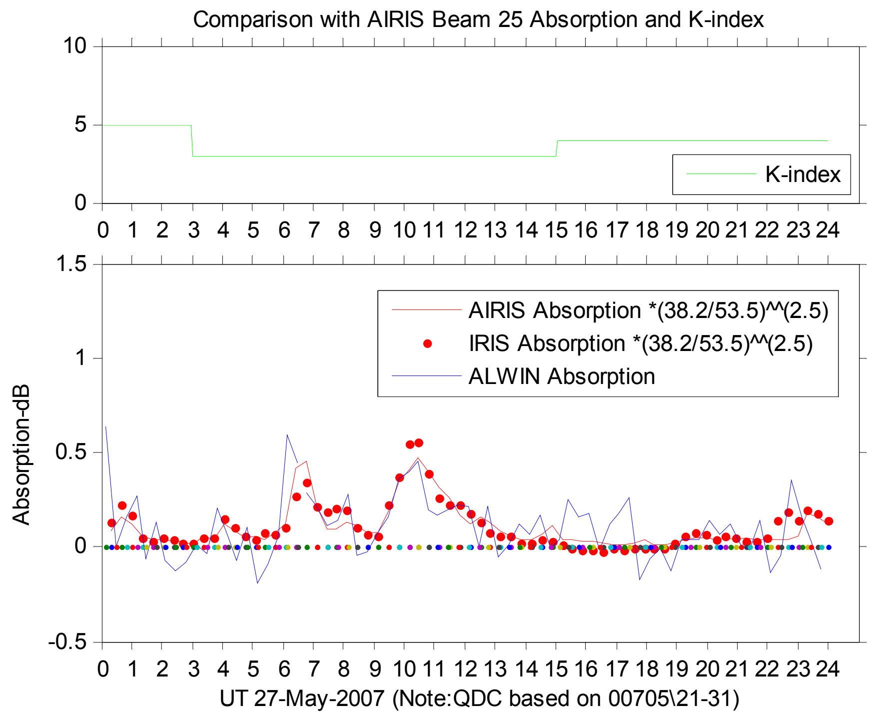

5.13. Cosmic noise absorption observed by ALWIN, AIRIS, and IRIS on My 27, 2007.

6. Conclusions

6.1. Discussion

The estimated ALWIN ionospheric absorption is generally in good agreement with that of the Riometer(s). One source of the difference between CNA's estimated by ALWIN and Riometer(s) can be that the observed volumes are different especially in case of the comparisons between ALWIN and IRIS. Having this in mind, we can expect that the absorptions estimated at different frequencies obey the equation $A(f) \sim f^{-2.5}$ in good approximation (see Figs. 5.2 to 5.13). Deviations from this rule can be also due to other reasons or artefacts like interference at the time of event, non-filtered interference/non-quiet data points affecting the QDC, lack of data (not enough number of data points) in one (corresponding time bin) or all of the time bins when estimating the QDC. The applied method depends on the amount of available applicable ALWIN data and degree of interference and solar activity around the event day.

Another important point is that we need to know a bit about the depth of ionization at the event time, especially when lack of data seems to be serious. If the ionization comes strongly down to heights as low as 50km heights, then the Event Day Curve will be filled by atmospheric echoes, rather than the cosmic noise, and then the output will not be the CNA. (In such cases we normally get negative CNA, stating that we have to use lower heights, if available). For example, in Fig. 5.2, only the two lowest heights (50 km, 50.3 km) are used in order to avoid the echoes of the heavy deep ionization. Detecting this situation from the method itself is usually possible, but some times getting the CNA becomes impossible if the data of lower heights is not available or applicable.

In the case of the January 2005 measurements, as seen in Figs. 5.2 to 5.4, presence of interference on the event times was the main problem. On 17th of January (Fig. 5.2), the whole afternoon is affected by interference, on 20th of January 2005, (Fig. 5.3) from 00:00 to 6:00 UT, and on 21st (Fig. 5.4), from 6:00 to 10:00 UT and from 18:00 to 24:00 UT. (In the figures, level 0 stands for no obvious interference at the corresponding time, and level

1 states that an obvious interference is present). These interferences cause error/difference in the estimated CNA of ALWIN at the corresponding times.

In the Oct/Nov 2003 estimations we have no interference time map, since there exists no data to be used as the basis for this part of data reduction. Another limitation is that we have only one week of applicable ALWIN data to work with (i.e. only 30 Oct to 5 Nov 2003) and the week is in a period which is not quiet. Here the lack of quiet data forced us to even include the data of times with K=4 (and hope that they will be reduced enough in the next steps of the reduction). We also had to use larger time bins (of one hour), to have enough data in the time bins, allowing us to estimate the Quiet Day Curve. An additional limitation was that ALWIN had a 600-m height step in 2003, and not a 300-m step as usual. Limited by the extremely enhanced ionizations down to 53 km and lower, (detected by ALWIN), here barely 5 heights were available (50, 50.6, 51.2, 51.8, 52.4, 53 km). Therefore the quality of the derived absorption data can be degraded by these limitations.

6.2. Summary

In this thesis a method has been developed to determine the cosmic radio noise power and its absorption (CNA) at 53.5 MHz by the ALWIN MST radar. The Quiet Day Curve, the non attenuated power curve, at 53.5 MHz is in good agreement with the empirical and simulated QDCs estimated by Friedrich et al. (2001). The estimated cosmic noise absorption values are in agreement with common-volume CNA observations by the AIRIS system on the Andoya island and by the IRIS system in Kilpisjärvi, Finland both operated at 38.2 MHz. The observations of the three different systems agree well in time and in magnitude of the absorption events if they are adjusted regarding the frequency dependence. The observed excessive absorption events are highly correlated with X ray fluxes and high energetic particle fluxes observed by GOES satellites as well as with geomagnetic disturbances. Reliable cosmic noise absorption data are obtained with the ALWIN radar for stronger events with absorption values larger about 0.3 dB due to the more variable RF background radiation at the ALWIN site.

At the *Event* times when interference is present on ALWIN, CNA estimation is not reliable, easily because the data of the event time is corrupt.

6.3. Further Works

The amount of ionospheric absorption at a given frequency depends mainly on the height distribution of ionization below 100 km. Cosmic radio noise power measured at two well separated frequencies (38.2 MHz and 53.5 MHz) provides the opportunity to estimate the height region where the most absorption occurred.

References

Armstrong R.J., Berkey F.T., and Melbye T.; The day to night absorption ratio in auroral zone riometer measurements, Planet. Space Sci. vol. 25, 1193, 1977

Brekke A.; Physics of the upper polar atmosphere, Wiley, 1997

Cane H. V., Von Rosenvinge T. T., Cohen C. M. S., and Mewaldt R. A.; Two components in major solar particle events, Geophysical Research Letters vol. 30 no. 12, 8017, 2003

Clilverd Mark A.; Modeling polar ionospheric effects during the October–November 2003 solar proton events, Radio Science, vol. 41, RS2001, doi:10.1029/2005RS003290, 2006

Drevin G.R. and Stoker P.H.; Determining riometer quiet day curves, 1. The Matrix Method, Radio Science, vol. 38, No. 2, 1024, 2003

Duffet-Smith P.; Practical astronomy with your calculator, Cambridge University Press, 2003

Friedrich M., Finsterbusch R., Torkar K.M., and Spocker P.; A further generalisation of the Sen and Wyller magneto–ionic theory. Advances in Space Research vol. 11 no.10, 105, 1991

Friedrich M., Harrich M., Torkar K.M., and Stauning P.; Quantitative measurements with wide beam riometers, Journal of Atmospheric and Solar-Terrestrial Physics vol. 64, no.3, 359, 2002

Hargreaves J. K., and Friedrich M.; The estimation of D-region electron densities from riometer data, Annales Geophysicae vol. 21; 603, 2003

Hargreaves J.K. ; A new method of studying the relation between ionization rates and radio wave absorption in Polar Cap Absorption events, Annales Geophysicae, vol. 23, 359, 2005

Hargreaves J. K.; The upper atmosphere and solar-terrstrial relations, Van Nostrand Reinhold, 1979

Harrich M., Friedrich M. , Marple S.R., and Torkar K.M.; The background absorption at high latitudes , Advances in Radio Science, 1; 1, 2003

Herndon J. M.; Nuclear georeactor origin of oceanic basalt 3He/4He, evidence, and implications, Proceedings of the National Academy of Sciences, vol. 100, no. 6, 3047, 2003

Hollenbach D. F. and Herndon J. M.; Deep-earth reactor: nuclear fission, helium, and the geomagnetic field, Proceedings of the National Academy of Sciences, vol. 98, no.20, 11085, 2001

Kavanagh A. J., Marple S. R., Honary F., McCrea I. W., and Senior A.; On solar protons and polar cap absorption: constraints on an empirical relationship, Annales Geophysicae, vol. 22, no. 4, 1133, 2004.

Kress B. T., Hudson M. K., Perry K. L., and Slocum P. L.; Dynamic modeling of geomagnetic cutoff for the 23–24 November 2001 solar energetic particle event, Geophysical Research Letters 31, L04 804, doi:10.1029/2003GL018599 ,2004.

Krucker S., and Lin R. P.; Two classes of solar proton events derived from onset time analysis, Astrophys. J., vol. 542, no.1, 61, 2000.

Latteck R. , Singer W., and Bardey H. ; The ALWIN MST Radar- Technical design and Performance, Proceedings 14th ESA Symposium on European Rocket and Balloon Programs and related Research, Potsdam, Germany, 31 May-3 June 1999, ESA SP -473, September 1999

Phelps A. V. and Pack J. L.; Electron collision frequencies in nitrogen and in the lower ionosphere, Phys. Rev. Lett., vol. 3, 340, 1959.

Rawer K.; Manual on ionospheric absorption measurements, World Data Center A- for Solar-Terrestrial Physics, NOAA, Boulder, Colorado, Report UAG 57, 1976

Rodger C.J., Clilverd M. A., Verronen P. T., Ulich Th., Jarvis M. J., and Turunen E.; Dynamic geomagnetic rigidity cutoff variations during a solar proton event, Journal Of Geophysical Research, vol. 111, A04222, doi:10.1029/2005JA011395, 2006.

Rosenberg T. J., Detrick D. L., Venkatesan D., and Van Bavel G.; A comparative study of imaging and broad beam riometer measurements, The effect of spatial structure on the frequency dependence of auroral absorption, Journal Of Geophysical Research, vol. 96, no. A10, 17793, 1991

Schroeter J., Heber B., and Kallenrode M.B.; Energetic particles in the atmosphere: a Monte Carlo simulation, COSPAR04, Advances in Space Research, vol. 37, no.8, 1597, 2006

Sen H.K., and Wyller A.A.; On the generalization of the Appleton–Hartree magneto–ionic formulas. Journal of Geophysical Research, vol. 65, 3931, 1960

Shea M. A., and Smart D. F.; A summary of major solar proton events, Solar Phys., vol. 127,no. 2, 297, 1990

Singer W., Holdsworth D., and Latteck R.; D-Region electron densities obtained by differential absorption and phase measurements with a 3-MHz Doppler Radar Geophysical Research Abstracts, vol. 7, 10045, 2005

Smart D. F., and Shea M. A.; Geomagnetic cutoff rigidity calculations at 50-year intervals between 1600 and 2000, Proc. ICRC 2003, 4201-4204, Universal, 2003

Space Environment Center report 2002–2003, U.S. Department of Commerce National Oceanic and Atmospheric Administration, February 2004

Versick S., Glatthor N., Stiller G., Reddmann T., and Ruhnke R.; Stratospheric hydrogen peroxide (H_2O_2) retrievals from MIPAS/ENVISAT for the episode of the October/November 2003 solar proton event, Geophysical Research Abstracts, vol. 9, 08542, 2007